Chapter 23B. Analysis of Imaging Spectrometer Data for the North Herat Area of Interest

By Todd M. Hoefen and Stuart A. Giles

Abstract

Imaging spectrometer data, from the HyMap sensor, collected over the North Herat area of interest (AOI) in western Afghanistan were analyzed with spectroscopic methods to identify the occurrence of selected material classes at the surface. Absorption features in the spectra of HyMap data were compared to a reference library of spectra of known materials. The coverage of this AOI is limited by the northern and western limits of the HyMap dataset. Thus, only the southeastern portion of the AOI has HyMap coverage. Carbonates were the main surface material in the North Herat AOI. Distinct patterns of chlorite or epidote, muscovite, illite, kaolinite, iron carbonate, and serpentine occur in localized patterns throughout the AOI. Many of the faulted areas in the northern region of the HyMap coverage have associated kaolinite and alunite. In the iron-bearing map, hematites dominate the valley floor between two east-west trending faults whereas ferrous iron "Fe^{2+} Fe^{3+} Type 2" occurs mainly along the southern border of the AOI and iron hydroxide occurs along the northern border of the southeast region. An analysis of HyMap data to detect gypsum was found to be effective in mapping the mineral in areas adjacent to a lacustrine gypsum prospect at Cheruland. Gypsum was also mapped in several other areas throughout the AOI where it was previously not known to occur and was found near areas of barite veins. The limestone known mineralized areas of Benosh Darrah, Darra-i-Chartagh, and Rod-i-Sanjur map within calcite-class minerals and are consistent with these types of prospects. The Karukh and Malumat clay prospects map within contiguous areas of calcite + montmorillonite. The Kushast and Taghab iron-skarn mineral occurrences may be associated with Fe^{2+} Fe^{3+} Type 2 minerals at Kushast and Fe^{3+} Type 1 minerals at Taghab.

23B.1 Introduction

Past studies of geologic data of Afghanistan revealed numerous areas with indications of potential mineral resources (Peters and others, 2007; Abdullah and others, 1977). Several of these areas were selected for follow-on studies using imaging spectroscopy to characterize surface materials. Imaging spectroscopy is an advanced type of remote sensing that is also known as hyperspectral remote sensing. One of those areas with potential mineral resources is the North Herat area of interest (AOI) in western Afghanistan, which is approximately 600 km west of Kabul (fig. 23B–1). The area is believed to have the potential for gypsum, barite, limestone, marble, brick clay, and iron-skarn prospects. To help assess these potential resources, high-resolution HyMap data were analyzed to detect the presence of selected minerals that may be indicative of past mineralization processes. This report contains the results of the spectroscopic data analyses and identifies sites within the North Herat AOI that warrant further investigation, especially, detailed geologic mapping, lithologic sampling, and geochemical studies.

23B.2 Data Collection and Processing

In 2007, imaging spectrometer data were acquired over most of Afghanistan as part of the U.S. Geological Survey (USGS) project "Oil and Gas Resources Assessment of the Katawaz and Helmand Basins." These data were collected to characterize surface materials in support of assessments of resources (coal, water, minerals, and oil and gas) and earthquake hazards in the country (King and others, 2010). Imaging spectrometers measure the reflectance of visible and near-infrared light from the

Earth's surface in many narrow channels, producing a reflectance spectrum for each image pixel. These reflectance spectra can be interpreted to identify absorption features that arise from specific chemical transitions and molecular bonds that provide compositional information about surface materials. Imaging spectrometer data can only be used to characterize the upper surface materials and not subsurface composition or structure. However, subsurface processes can be indicated by the distribution of surface materials.

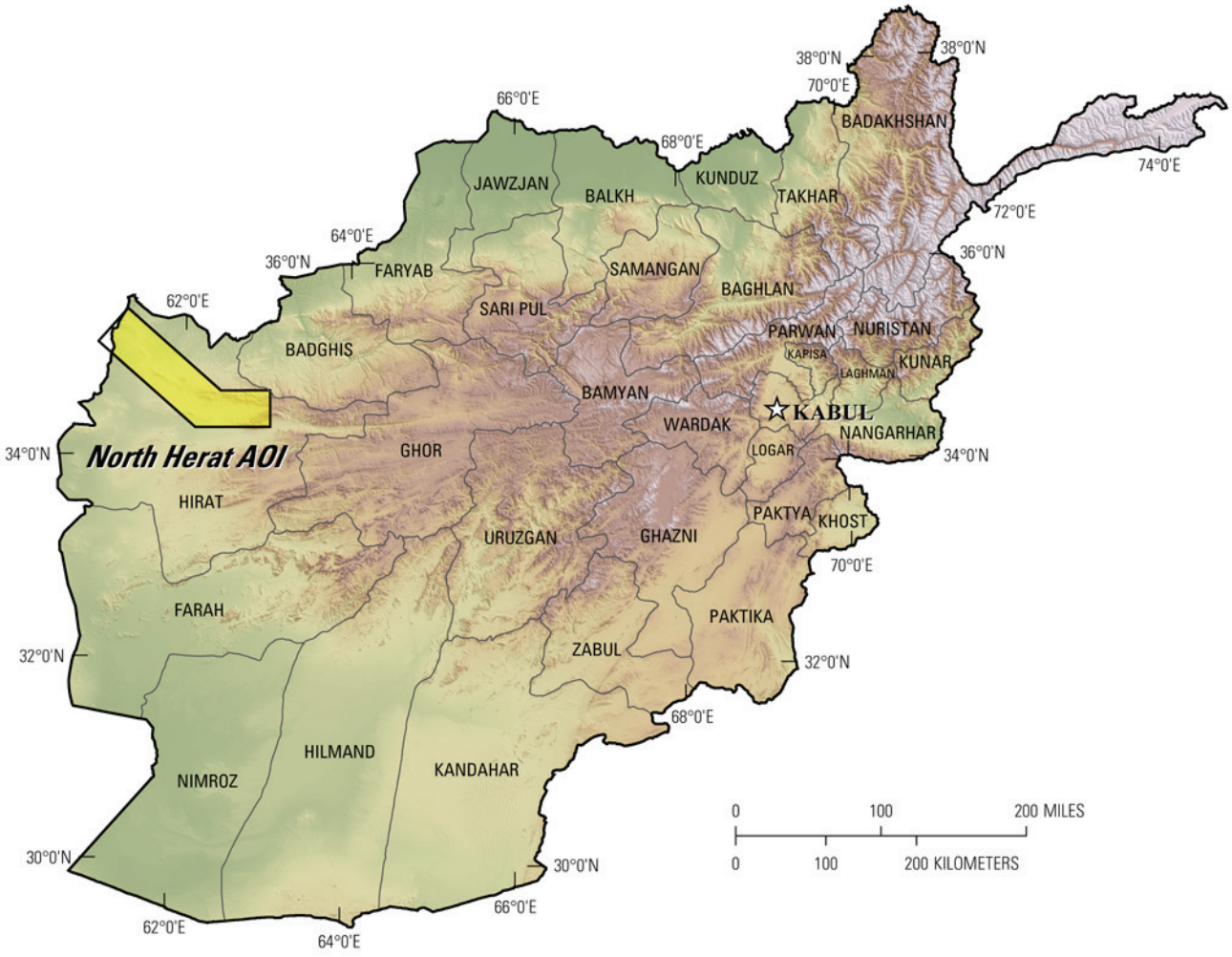

Figure 23B–1. Index map of the North Herat area of interest, northeastern Afghanistan.

23B.2.1 Collection of Imaging Spectrometer Data

The HyMap imaging spectrometer (Cocks and others, 1998) was flown over Afghanistan from August 22 to October 2, 2007 (Kokaly and others, 2008). HyMap has 512 cross-track pixels and covers the wavelength range 0.43 to 2.48 microns (μm) in 128 channels. The imaging spectrometer was flown on a WB-57 high-altitude aircraft at approximately 50,000 ft. There were 207 standard data flight lines and 11 cross-cutting calibration lines collected over Afghanistan for a total of 218 flight lines, covering a surface area of 438,012 km^2 (Kokaly and others, 2008). Data were received in scaled radiance (calibrated to National Institute of Standards and Technology reference materials). Before processing, four channels that had low signal-to-noise and (or) were in wavelength regions that overlapped between detectors were removed from the HyMap data. Each flight line was georeferenced to Landsat Thematic Mapper (TM) imagery in UTM projection (Davis, 2007).

23B.2.2 Calibration

HyMap data were converted from radiance to reflectance using a multi-step process. This calibration process removed the influence of the solar irradiance function, atmospheric absorptions, and residual instrument artifacts, resulting in reflectance spectra that have spectral features that arise from the material composition of the surface. Because of the extreme topographic relief and restricted access to ground-calibration sites, modifications to the typical USGS calibration procedures were required to calibrate the 2007 Afghanistan HyMap dataset (Hoefen and others, 2010). In the first step of the calibration process, the radiance data were converted to apparent surface reflectance using the radiative transfer correction program Atmospheric CORrection Now (ACORN; ImSpec LLC, Palmdale, Calif.). ACORN was run multiple times for each flight line, using average elevations in 100-m increments, covering the range of minimum to maximum elevation within the flight line. A single atmospherically corrected image was assembled from these elevation-incremented ACORN results. This was done by determining the elevation of each HyMap pixel and selecting the atmospherically corrected pixel from the 100-m increment closest to that elevation.

Each assembled atmospherically corrected image was further empirically adjusted using ground-based reflectance measurements from a ground-calibration site. Spectra of five ground-calibration sites were collected in Afghanistan: field spectra from Kandahar Air Field, Bagram Air Base, and Mazar-e-Sharif Airport, as well as, laboratory spectra of soil samples from two fallow fields in Kabul. These were used to calculate empirical correction factors using the pixels of atmospherically corrected HyMap data in the flight lines that passed over the sites. The empirical correction from the closest calibration site to each flight line was applied.

To further improve the data quality, an additional calibration step was taken to address the atmospheric differences caused, in part, by the large distances from calibration sites to where the HyMap data were acquired. The large distances were a result of the lack of safe access to ground-calibration sites. The duration of the airborne survey and variation in time of day during which flight lines were acquired also resulted in differences in atmospheric conditions between standard flight lines and lines over ground-calibration sites. Over the course of the data collection, the sun angle, atmospheric water vapor, and atmospheric scattering differed for each flight line. To compensate for this, cross-cutting calibration flight lines over the ground-calibration areas were acquired (Kokaly and others, 2008) and used to refine data quality of standard data lines. A multiplier correction for each standard data line, typically oriented north-south, was derived using the pixels of overlap with the well-calibrated cross-cutting line that intersected it, subject to slope, vegetation cover, and other restrictions on pixel selection (Hoefen and others, 2010). As a result, the localized cross-calibration multiplier, derived from the overlap region, corrected residual atmospheric contamination in the imaging spectrometer data that may have been present after the ground-calibration step.

23B.2.3 Materials Maps and Presentation

After the calibration process, the reflectance data were georeferenced and then analyzed using the Material Identification and Characterization Algorithm (MICA), a module of the USGS Processing Routines in IDL (Interactive Data Language) for Spectroscopic Measurements (PRISM) software (Kokaly, 2011). The MICA analysis compared the reflectance spectrum of each pixel of HyMap data to entries in a reference spectral library of minerals, vegetation, water, and other materials. The HyMap data were compared to 97 reference spectra of well-characterized mineral and material standards. The best spectral match to each pixel was determined and the results were clustered into classes of materials discussed below. The resulting maps of material distribution, resampled to a 23 × 23 meter square pixel grid, were mosaicked to create thematic maps of surface mineral occurrences over the full dataset covering Afghanistan.

MICA was applied to HyMap data twice in order to present the distribution of two categories of minerals that are naturally separated in the wavelength regions of their primary absorption features. MICA was applied using the subset of minerals with absorption features in the visible and near-infrared wavelength region, producing a 1-μm map of iron-bearing minerals and other materials (King, Kokaly, and others, 2011), and again using the subset of minerals with absorption features in the shortwave infrared, producing a 2-μm map of carbonates, phyllosilicates, sulfates, altered minerals, and other materials (Kokaly and others, 2011). For clarity of presentation, some individual classes in these two maps were bundled by combining selected mineral types (for example, all montmorillonites or all kaolinites) and representing them with the same color in order to reduce the number of colors required to represent the mineral classes.

The iron-bearing minerals map has 28 classes. Iron-bearing minerals with different mineral compositions but similar broad spectral features are difficult to classify as specific mineral species. Thus, generic spectral classes, including several minerals with similar absorption features, such as Fe^{3+} Type 1 and Fe^{3+} Type 2 are depicted on the map. The 2-μm map of carbonates, phyllosilicates, sulfates, and altered minerals has 32 classes. Minerals with slightly different chemical compositions but comparable spectral features are less easily discriminated; thus, some identified classes consist of several minerals with similar spectra, such as the chlorite or epidote class. When comparisons with reference spectra resulted in no viable match, a designation of "not classified" was assigned to a pixel.

23B.3 Geologic Setting of the North Herat Area of Interest

The North Herat AOI is within the Hirat Province in western Afghanistan, covering 9,684 km^2. The contrast-enhanced stretch of the natural-color composite of Landsat TM bands in figure 23B–2 provides a general overview of the North Herat AOI terrain and is useful for understanding the general characteristics and distribution of surficial material including rocks and soil, unconsolidated sediments, vegetation, and hydrologic features.

23B.3.1 Topography

Elevations in the North Herat AOI range from 536 to 3,543 m (fig. 23B–3). The lowest areas within the North Herat AOI are in the plains of the northwestern region of the AOI. The highest areas are found in the central and eastern regions of the AOI. The three population centers within the AOI are the province center of Herat (also spelled Hirat) and the two district centers of Gulran and Karukh.

23B.3.2 Lithology and Structure

Two major fault systems run through the AOI (fig. 23B–4; Doebrich and Wahl, 2006; Abdullah and Chmyriov, 1977). The first is an east-west trending fault system that runs parallel to the southern edge of the AOI approximately 10 km north of the southern border of the AOI. The other is a northwest-southeast trending fault system that starts in the northern region of the AOI, and as it trends south the fault system becomes more east-west trending.

Rocks in the North Herat AOI range in age from Proterozoic to Recent (fig. 23B–4). Intrusive rocks of Proterozoic and Late Triassic age occur within the AOI. The Proterozoic intrusive rocks occur in the southeastern corner of the region. Only three small occurrences of Late Triassic intrusives occur in the south-central region of the North Herat AOI. In the south-central region, Early Proterozoic stratified rock units are surrounded by much younger Miocene and Quaternary units. Carboniferous, Permian, and Triassic stratified rocks occur at higher elevations in the eastern region with occasional units occurring along the fault system to the northwest. Cretaceous rocks occur along the northern border of the northeastern region of the AOI. Cenozoic stratified units occur throughout the North Herat AOI and are usually limited to the lower elevations.

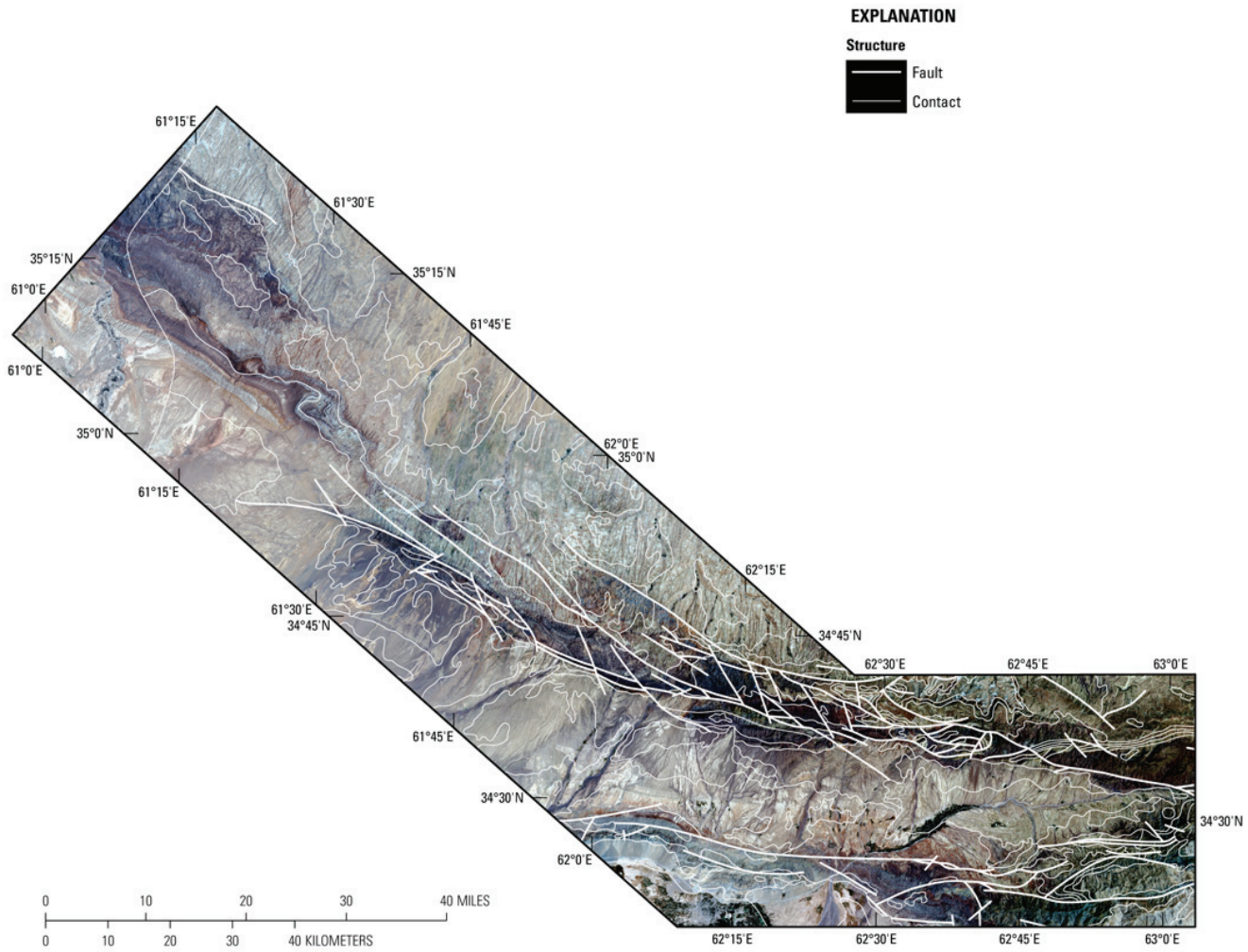

Figure 23B–2. Contrast-enhanced Landsat Thematic Mapper natural-color image of the North Herat area of interest. Geologic contacts and faults from Doebrich and Wahl (2006) and Abdullah and Chmyriov (1977).

23B.3.3 Known Mineralization

Figure 23B–5 shows 13 locations where mineralization with a potential for mineral resource development may exist (Peters and others, 2007; Abdullah and others, 1977; Doebrich and Wahl, 2006). A number of different types of mineral prospects, particularly limestone, clay, gypsum, and barite, are present within the North Herat AOI. The mineralogical characteristics of the mineralized locations are summarized in table 23B–1. There are also occurrences of iron (Fe) skarns, a polymetallic vein, and vein barite.

The largest barite and gypsum prospect is the Sangilyn prospect, which covers an area of over 3 km^2 and is hosted in Eocene to Oligocene volcanic and sedimentary rocks and contains three mineralized zones. Each of the zones is up to 2,500 m long and 200 to 700 m wide, and these are characterized by 24 major and numerous minor fracture-filled barite veins that are 70 to 1,000 m long and 0.4 to 5.7 m thick. A number of different barite types are present including (1) monomineralic, coarse-crystalline barite that is 0.5 to 5.5 m thick and grades 80 to 98.6 weight percent barite, (2) fine-grained barite that is present along chilled contacts between the enclosing veins and host rock that are 0.1 to 0.7 m thick and grade 75 to 94 weight percent barite, (3) coarse-grained mixtures of barite and calcite, (4) barite associated with fault breccia, and (5) disseminated barite. The barite veins are usually monomineralic and also may contain witherite, galena, sparse disseminated chalcopyrite and pyrite, as well as small quartz crystals, calcite, malachite, and limonite. Resources calculated for the

prospect were 1,493,000 tonnes barite when the mine was active in 1977 (Peters and others, 2007; Doebrich and Wahl, 2006; Abdullah and others, 1977).

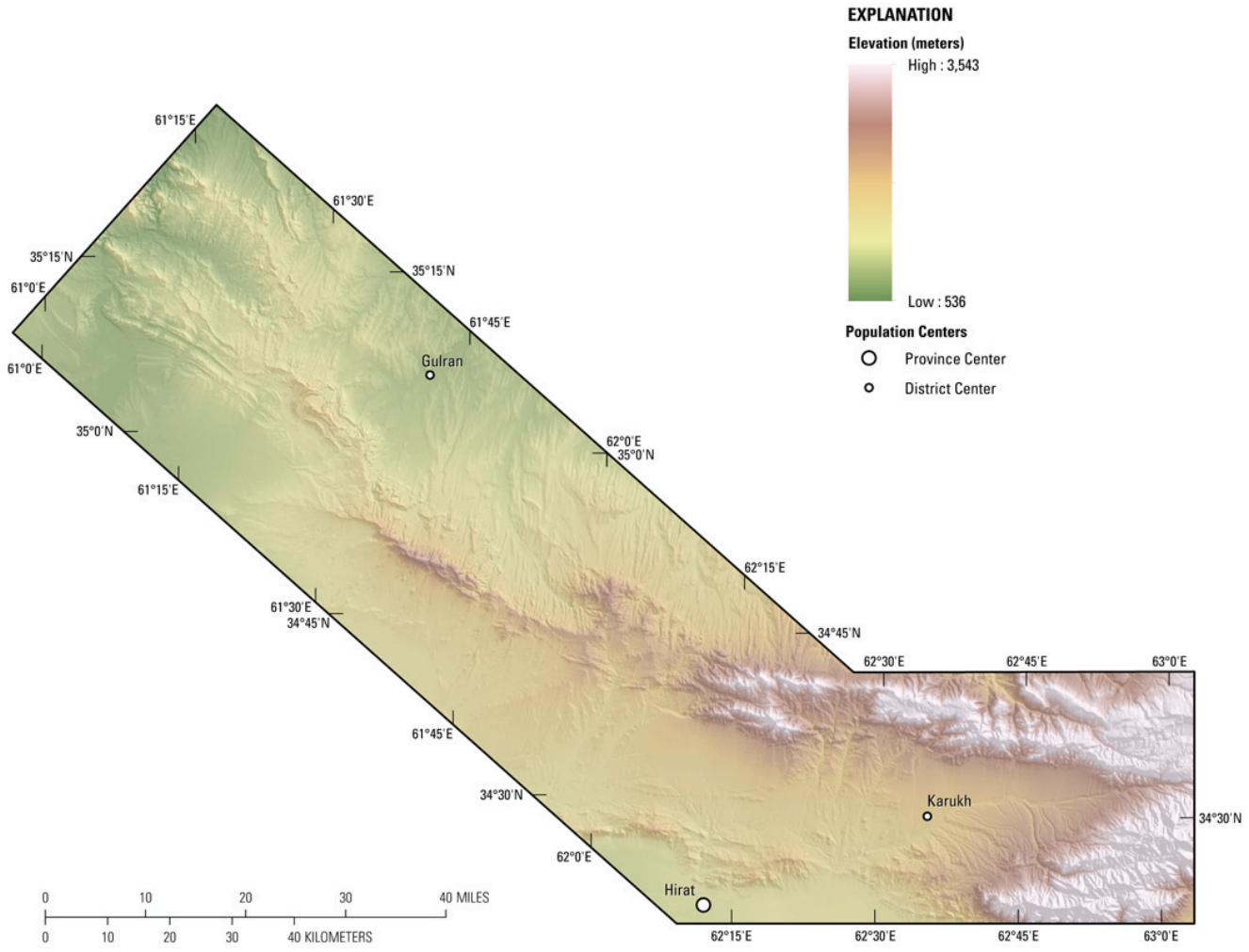

Figure 23B–3. Elevations and topography of the North Herat area of interest.

Three limestone prospects are being investigated for use by a cement plant in the North Herat subarea. The three prospects are the Rod-i-Sanjur, Darra-i-Chartagh and Benosh Darrah. The Benosh Darrah prospect is located near lat 34°34'30"N., long 62°46'20"E. The prospect occurs in Lower Triassic limestones that are 464 m thick with the outcrop covering an area of 3 km^2. The Darra-i-Chartagh prospect is located near lat 34°26'20"N., long 62°46'00"E. It also occurs in Lower Triassic limestone beds that are up to 460 m thick and extends 5 to 6 km in length. The limestone is light colored, compact, fine-grained, occasionally oolitic and pseudo-oolitic, bearing fine organic detritus. At places the rock is contaminated with silty or sandy material making up 8 volume percent of the rock and consisting of quartz, feldspar, and rarely, altered felsite grains. The Rod-i-Sanjur prospect located near lat 34°26'01"N., long 62°44'00"E. is 410 m thick and occurs in Middle–Upper Triassic limestone. It is fine-grained and bedded at the base and fine-grained to aphanitic, compact, with a conchoidal fracture, vaguely bedded to massive at the top (Peters and others, 2007; Doebrich and Wahl, 2006; Abdullah and others, 1977).

Additional barite occurrences in the North Herat AOI are the Gardani-Burida prospect and the Gulron barite occurrence. The Gardani-Burida prospect contains five milky-white to pink, coarse- to fine-grained, lenticular barite-bearing bodies that are 5 to 20 m long and 0.2 to 0.6 m thick. The Gulron barite occurrence lies along a fault zone that is 30 to 700 m long and 0.15 to 0.7 m thick and cuts Eocene

sedimentary rocks. The Gulron prospect contains eight barite veins with transparent Iceland spar crystals that are as large as 10 × 20 cm,15 barite-calcite veins, and two calcite veins (Peters and others, 2007; Doebrich and Wahl, 2006; Abdullah and others, 1977). The Gulron prospect occurs outside of our mapped area.

Within the Cenozoic basin are the Karukh and Malumat occurrences of clay. The Karukh prospect is located near lat 34°30'26"N., long 62°34'14"E. The prospect consists of Quaternary clay applicable for brick manufacture. The Malumat prospect is located near lat 34°29'03"N., long 62°43'28"E. The area is underlain by Quaternary clays varying in lime content and rich in silty and sandy material (Peters and others, 2007; Doebrich and Wahl, 2006; Abdullah and others, 1977).

Two iron occurrences, the Taghab and Kushast prospects, lie on the eastern side of the North Herat AOI. The Taghab iron prospect is located near lat 34°36'11"N., long 62º57'12"E. Lenses and irregular bodies of magnetite ore in epidote-garnet skarns are 1 to 3 m thick and are formed in Upper Permian rocks at their contact with a small granodiorite massif of Late Triassic age. Magnetite is partially replaced by martite. Gangue materials at this occurrence include epidote and garnet. The Kushast prospect is located near lat 34°28'05"N., long 62°59'26"E. Here a concordant hematite-magnetite ore body is confined to skarned shale and carbonate of early Carboniferous age at their contact with a small granitic massif of Late Triassic age. Its width is 4.5 m and is 150 m long (Peters and others, 2007; Doebrich and Wahl, 2006; Abdullah and others, 1977).

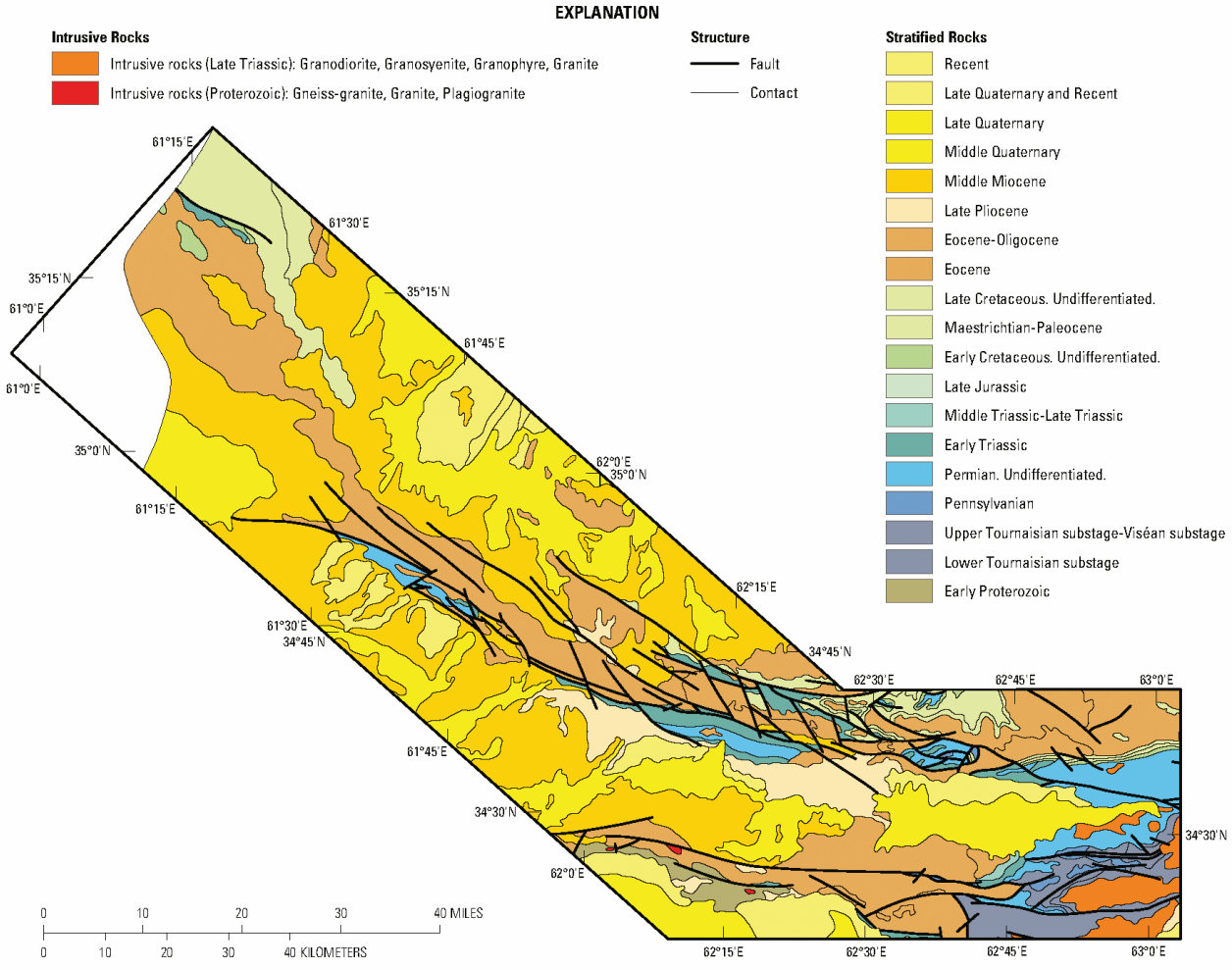

Figure 23B–4. Geologic map of the North Herat area of interest from the geologic map of Afghanistan (Doebrich and Wahl, 2006; Abdullah and Chmyriov, 1977).

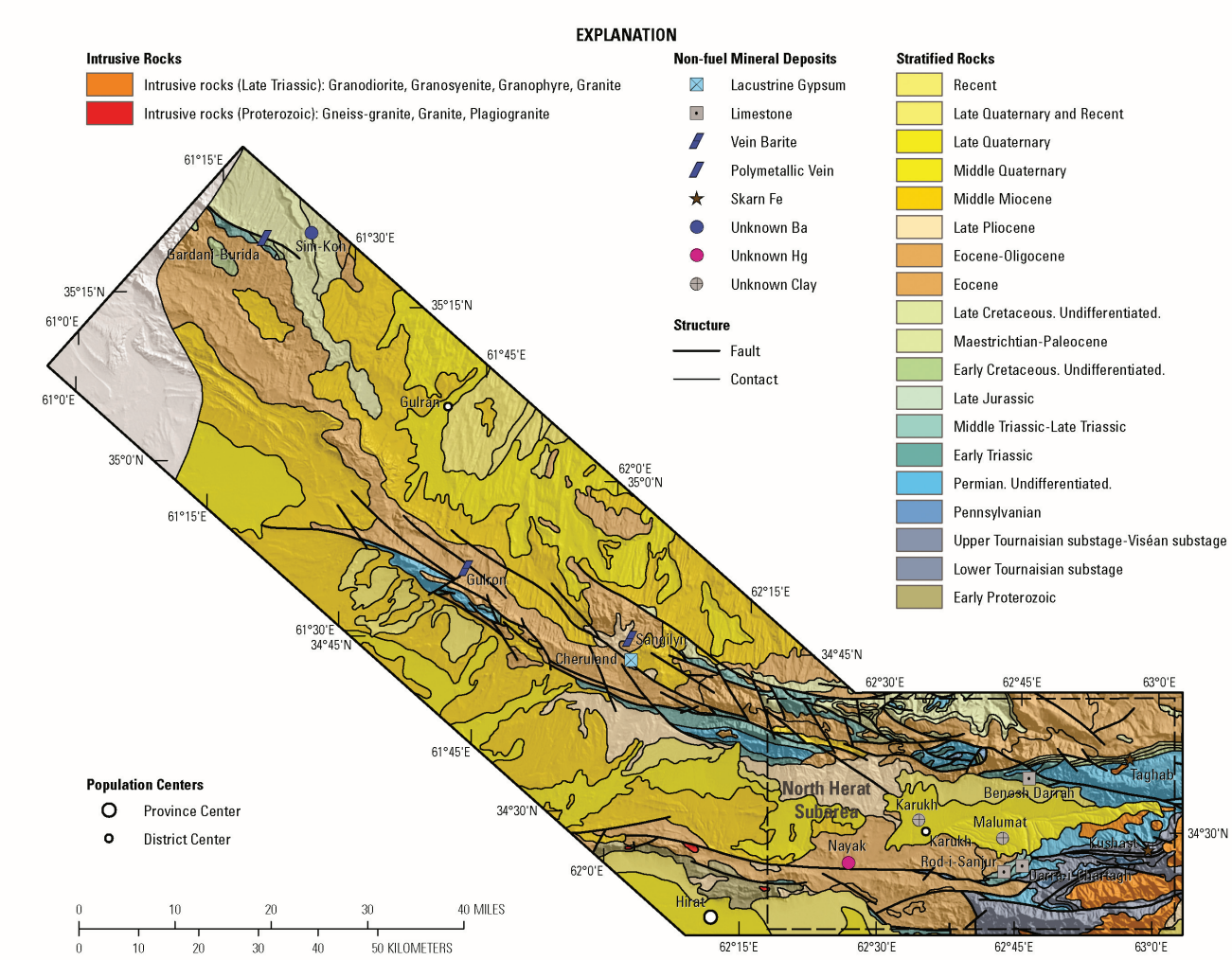

Figure 23B–5. Sites of known mineralization by deposit type (Peters and others, 2007) on the geologic map of the North Herat area of interest from the geologic map of Afghanistan (Doebrich and Wahl, 2006; Abdullah and Chmyriov, 1977). The dashed line in this figure shows the North Herat subarea boundary.

23B.3.4 Data Limitations

It should be noted that geographic registration between various datasets is not always possible, because of differences in collection methods and resolution. The geographic accuracy and quality of each dataset is limited by the original source. Significant efforts were made to ensure the geographic accuracy of the HyMap data. However, exact registration between previously published known mineral occurrences, fault traces, geologic units, and structural boundaries in comparison to the HyMap data may not be ideal. To resolve additional details, the digital versions of these maps can be viewed at higher spatial resolution than what is possible in a single-page printed map.

23B.4 Mineral Maps of the North Herat Area of Interest

Analysis of the HyMap imaging spectrometer data of the North Herat AOI using spectroscopic methods resulted in the identification of a wide variety of minerals exposed at the surface. Although the occurrence of certain minerals may suggest that mineralization processes may have once operated in the area, many of the minerals that were identified are also common rock-forming minerals or minerals that can be derived from the weathering of a wide variety of rock types. Consequently, the distribution patterns of the identified minerals and the geologic context in which they occur are extremely important

in understanding the causes of mapped mineral occurrences and evaluating the potential for related mineral deposits. Abundant vegetation, which masks surficial minerals, reduced the utility of the imaging spectrometer data in a few areas in the North Herat AOI.

Figures 23B–6 and 23B–7 depict the distribution of the carbonates, phyllosilicates, sulfates, altered minerals, and other materials (32 possible classes) and the iron-bearing minerals (28 possible classes) for the entire North Herat AOI.

Table 23B–1. Sites of known mineralization in the North Herat area of interest (Peters and others, 2007; Abdullah and Chmyriov, 1977).
[Cu, copper; Fe, iron; Ba, barium; Hg, mercury

Name	Deposit type	Major commodity	Alteration	Mineralogy	Gangue
Cheruland	Lacustrine gypsum	Gypsum	No data	Gypsum	No data
Rod-i-Sanjur	Limestone	Limestone	No data	No data	No data
Darra-i-Chartagh	Limestone	Limestone	No data	No data	No data
Benosh Darrah	Limestone	Limestone	No data	No data	No data
Sim-Koh	Polymetallic vein	Cu	No data	Malachite; azurite; cuprite; chalcocite	No data
Kushast	Skarn Fe	Fe	Skarn alteration	Magnetite; hematite	No data
Taghab	Skarn Fe	Fe	Skarn alteration of garnet-epidote facies	Magnetite; martite	Epidote; garnet
Gardani-Burida	Unknown Ba	Ba	Baritization	Barite	No data
Malumat	Unknown clay	Brick clay	No data	No data	No data
Karukh	Unknown clay	Brick clay	No data	No data	No data
Nayak	Unknown Hg	Hg, Cu	No data	Cinnabar; chalcocite; chalcopyrite; bornite; malachite	No data
Sangilyn	Vein barite	Ba	Baritization; calcite alteration	Barite; witherite; chalcopyrite; pyrite; galena	Quartz; calcite
Gulron	Vein barite	Ba	Baritization; calcite alteration	Barite	Calcite

The map of carbonates, phyllosilicates, sulfates, altered minerals, and other materials (fig. 23B–6) shows that the carbonate mineral groups cover most of the North Herat AOI. Pixels matching pure muscovite or illite spectra occur over large contiguous areas throughout the region. Distinct patterns of chlorite or epidote occur in the southeast region of the AOI. Iron carbonate and the kaolinite mineral groups form large coherent concentrations of pixels in the south-central and northeast regions respectively.

In the iron-bearing minerals map, the Fe^{2+} Fe^{3+} Type 2 class dominates the southern border of the AOI and occurs within rocks of many different ages covering a long span of geologic time. Most of the Fe^{2+} Fe^{3+} Type 2 occurs south of the southernmost fault system and is generally found in the higher elevations within the area. Fe^{2+} Fe^{3+} Type 2 minerals can be seen as blue-gray-colored rocks in the TM image (see fig. 23B–2). A small area of Fe^{2+} Fe^{3+} Type 2, Fe^{3+} Type 1, epidote, and hematite occurs within Upper Cretaceous rocks near lat 34°40'52"N., long 62º36'48"E. Fe^{2+} Fe^{3+} Type 1 occurs within lower Tournaisian rocks near fault lines in the southeast corner of the AOI. The Kushast and Taghab Fe-skarn prospects map near regions of Fe^{2+} Fe^{3+} Type 2 at Kushast and Fe^{3+} Type 1 at Taghab (see fig. 23B–7). The iron oxides and iron hydroxides will be discussed in a later chapter.

Because of the large number of classes represented and the subtleties of the distribution patterns represented in these image maps, it is instructive to display these results as a series of image maps each depicting a selected group of minerals that are mineralogically related or commonly occur together in special geologic environments (figs. 23B–8 to 12). Figure 23B–8 shows the distribution of carbonate minerals in the North Herat AOI, whereas figure 23B–9 shows where clay minerals and micas occur. The distribution of iron-oxide and iron-hydroxide minerals is displayed in figure 23B–10. Minerals

commonly found in hydrothermally altered rocks are mapped in figure 23B–11, and secondary minerals often associated with mineralized and (or) weathered rocks are mapped in figure 23B–12.

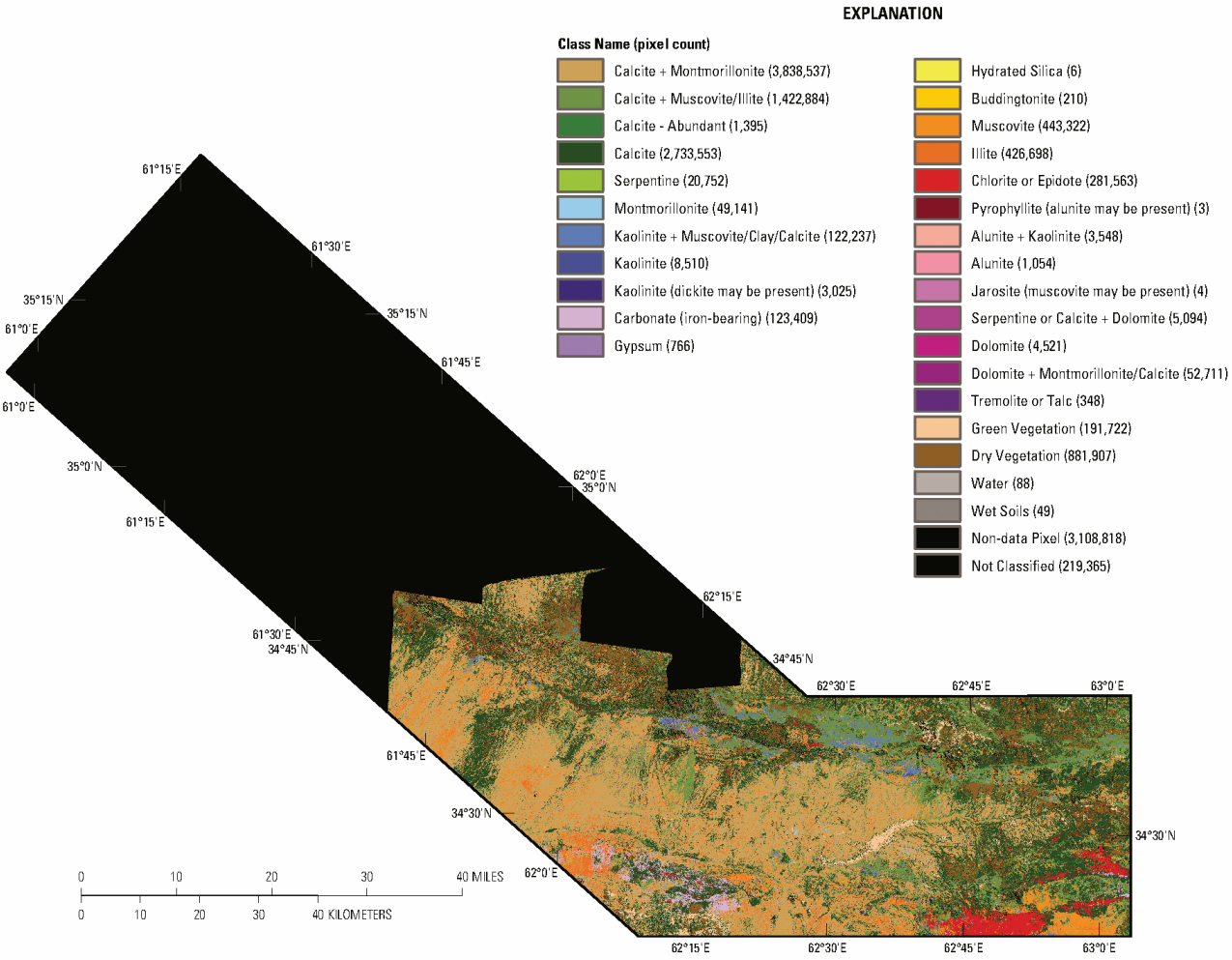

Figure 23B–6. Map of carbonates, phyllosilicates, sulfates, altered minerals, and other materials derived from HyMap data in the North Herat area of interest.

23B.4.1 Carbonate Minerals

Carbonate minerals, either calcite, calcite + montmorillonite or calcite + muscovite/illite, were mapped over a large majority of the North Herat AOI (fig. 23B–8). In general, the carbonates were mapped throughout the AOI and within almost every geologic unit. Iron carbonates were mapped in two regions. One large occurrence was mapped in the south-central region of the North Herat AOI, mainly in Early Proterozoic stratified rocks with a significant portion of the pixels near the contact of the Early Proterozoic stratified rocks and much younger Cenozoic rocks (lat 34°24'42"N., long 62°14'15"E.). Several faults occur within the area as well. This area warrants further investigation in future studies and is shown in more detail in another report (King, Johnson, and others, 2011). The second region has iron carbonate mapped in several large clusters throughout the lower Tournaisian substage rocks and into adjacent Late Triassic intrusive rocks in the southeast corner of the AOI (lat 34°26'26"N., long 63°00'46"E. and lat 34°24'33"N., long 63°02'52"E.). In two of the clusters, the iron carbonates also map along a fault line. Dolomite and serpentine or calcite + dolomite were mapped throughout the AOI but did not map in coherent clusters. The limestone known mineralized area of Benosh Darrah occurs within a calcite + muscovite/illite unit in the western region of the AOI. The Darra-i-Chartagh and Rod-i-Sanjur

limestone occurrences map within the calcite class and are consistent with these type prospects. The gangue minerals for the Sangilyn barite prospect are listed as quartz and calcite (Abdullah and others, 1977; Doebrich and Wahl, 2006), and the HyMap data does show that the mineral occurrence is located in calcite-rich rocks.

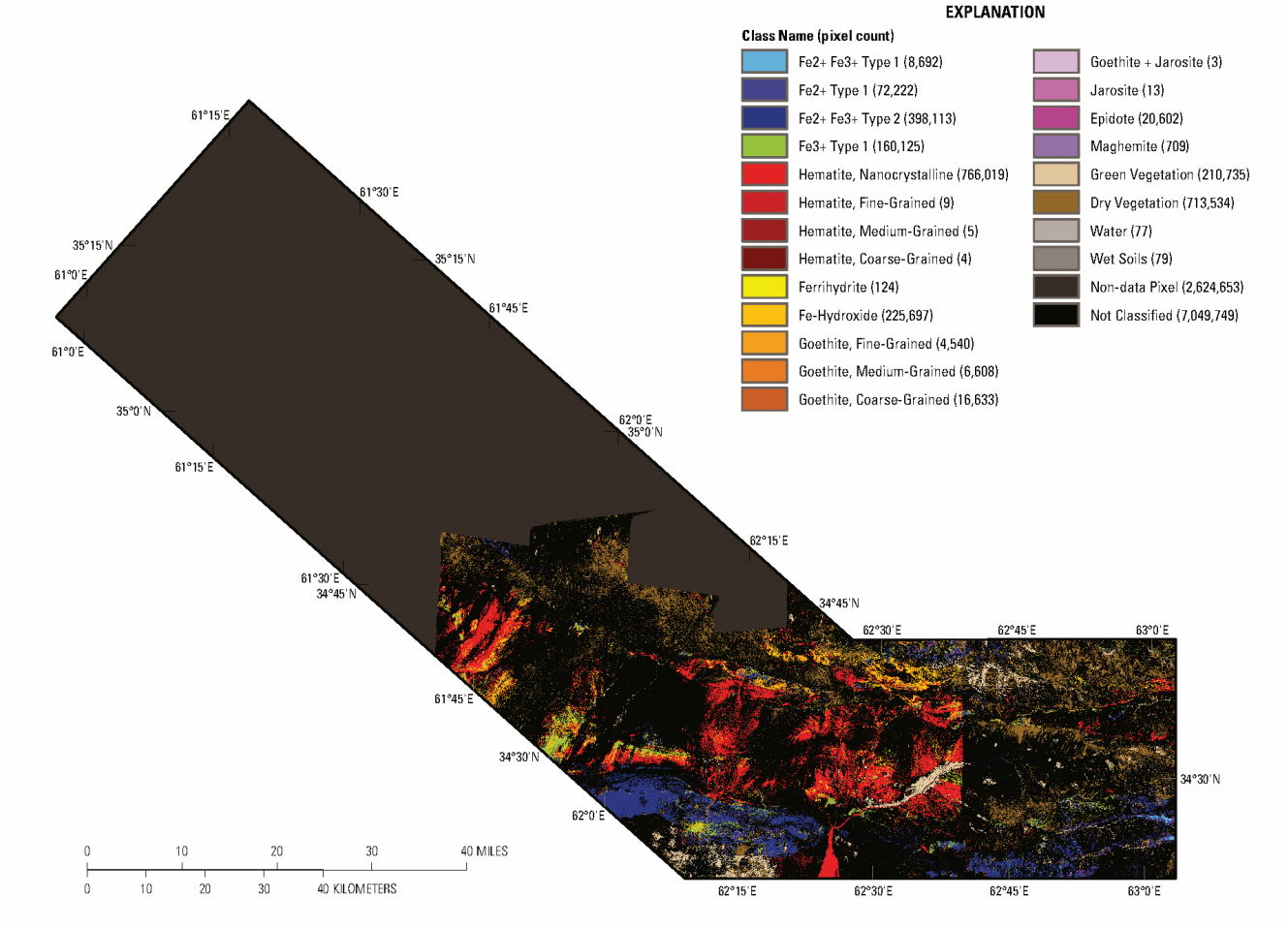

Figure 23B–7. Map of iron-bearing minerals and other materials derived from HyMap data in the North Herat area of interest.

23B.4.2 Clays and Micas

Calcite + montmorillonite and calcite + muscovite/illite dominate the clays and micas map in figure 23B–9. These two classes map throughout the AOI in rocks of many different ages. The calcite + muscovite/illite generally maps at the higher elevations in the northeast region of the AOI in Cretaceous and Cenozoic age rocks. Calcite + montmorillonite typically occurs at lower elevations in younger rocks. Pixels matching pure muscovite or illite spectra are dispersed over large areas in the AOI. In the southeast corner of the AOI, a large occurrence of pixels mainly mapping as muscovite is found in Late Triassic intrusive rocks. In the south-central regions of the AOI, illite maps in a contiguous area over several different ages and types of rocks. The largest occurrences of chlorite or epidote are found within the lower Tournaisian substage stratified rocks in the southeast corner of the AOI. Smaller occurrences of chlorite or epidote are found within Lower Triassic rocks in the central region and are generally found along the geologic boundary on a fault line. In the south-central region, chlorite or epidote maps near a fault line in Early Proterozoic rocks. This suggests that the accuracy of the fault map may be improved with the HyMap data.

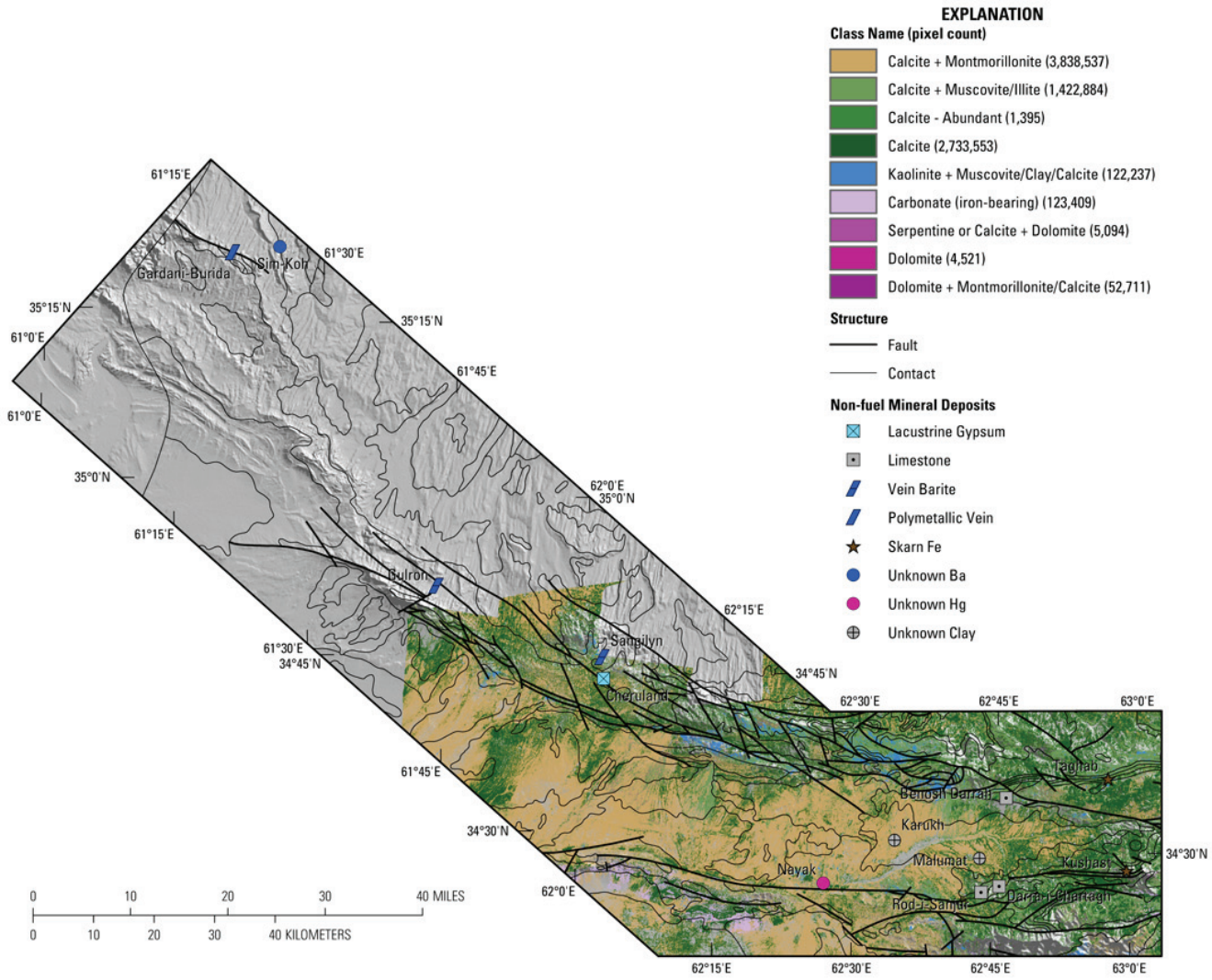

Figure 23B–8. Map of distribution of carbonate minerals derived from HyMap data in the North Herat area of interest.

Montmorillonite pixels are spatially scattered over the AOI with one small enriched concentration occurring along the contact zone of late Pliocene and Eocene-Oligocene age rocks in the central region of the AOI (lat 34°35'36"N., long 62°26'04"E.). The kaolinite classes primarily occur within Early Triassic age rocks in the central region of the North Herat AOI, although kaolinite can be found in Pennsylvanian age rocks in several locations. There are many faults within this region and kaolinite does occur in several other areas along fault traces. This is important because the kaolinite in this region could be associated with hydrothermal activity along a fault. The alunite + kaolinite class occurs in a large area within an Early Triassic age unit. This occurrence is located near lat 34°39'00"N., long 62°12'05"E., and warrants further investigation. Four smaller occurrences of alunite + kaolinite located at lat 34°43'53"N., long 61°50'23"E., lat 34°35'04"N., long 62°38'27"E., lat 34°25'55"N., long 62°34'54"E., and lat 34°37'38"N., long 62°34'18"E., should also be investigated. These areas are shown in more detail by King, Johnson, and others (2011). The Malumat and Karukh clay prospects, with the major commodity listed as Brick Clay, occur in areas where montmorillonite has been mapped both as its own independent class and in montmorillonite + calcite, which is consistent with the commodity (Abdullah and others, 1977; Doebrich and Wahl, 2006).

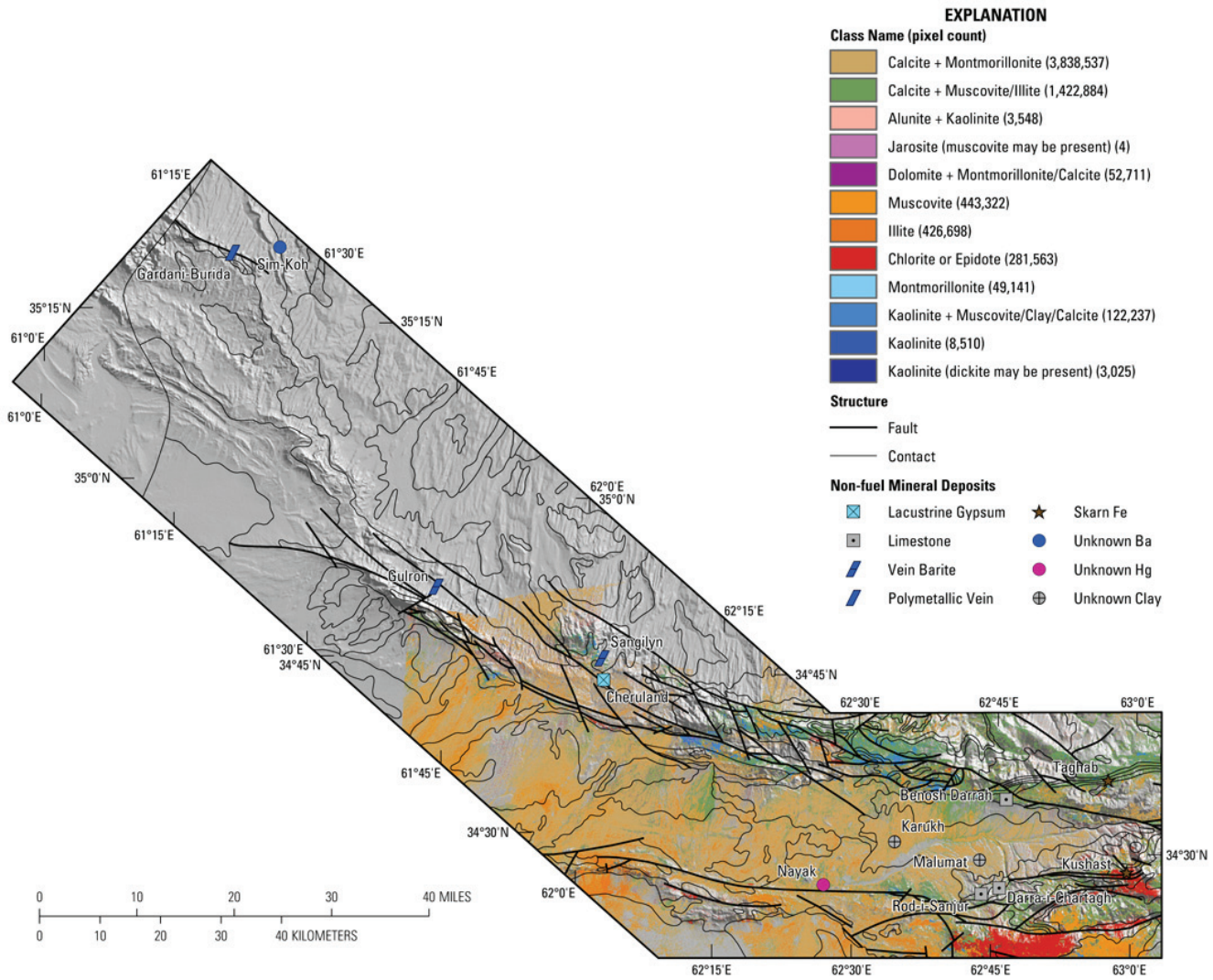

Figure 23B–9. Map of distribution of clay and mica minerals derived from HyMap data in the North Herat area of interest.

23B.4.3 Iron Oxides and Hydroxides

The North Herat AOI contains large areas of hematite in the southern region of the area (fig. 23B–10). The hematite is bounded on the north and south by two major fault lines and in general maps within the lower elevations. Iron hydroxide, with smaller amounts of goethite dispersed throughout it, is found across the AOI but is mainly found in a highly fractured zone in the north-central region. Smaller amounts of Fe-hydroxide are also found within Cenozoic rocks in the western edge of the HyMap data within hematite occurrences. Occurrences of epidote are found dispersed throughout the Early Proterozoic rocks in the south-central region and within Upper Cretaceous undifferentiated stratified rocks along the north-central border of the AOI. A sharp boundary can be seen in the hematite in the eastern region of the North Herat AOI in figures 23B–10 and 23B–7. This is most likely caused by different atmospheric conditions on the two different days of data acquisition and caused by the uncorrected scattering in the eastern- most lines of the AOI, and thus, hematite could easily extend into the eastern area.

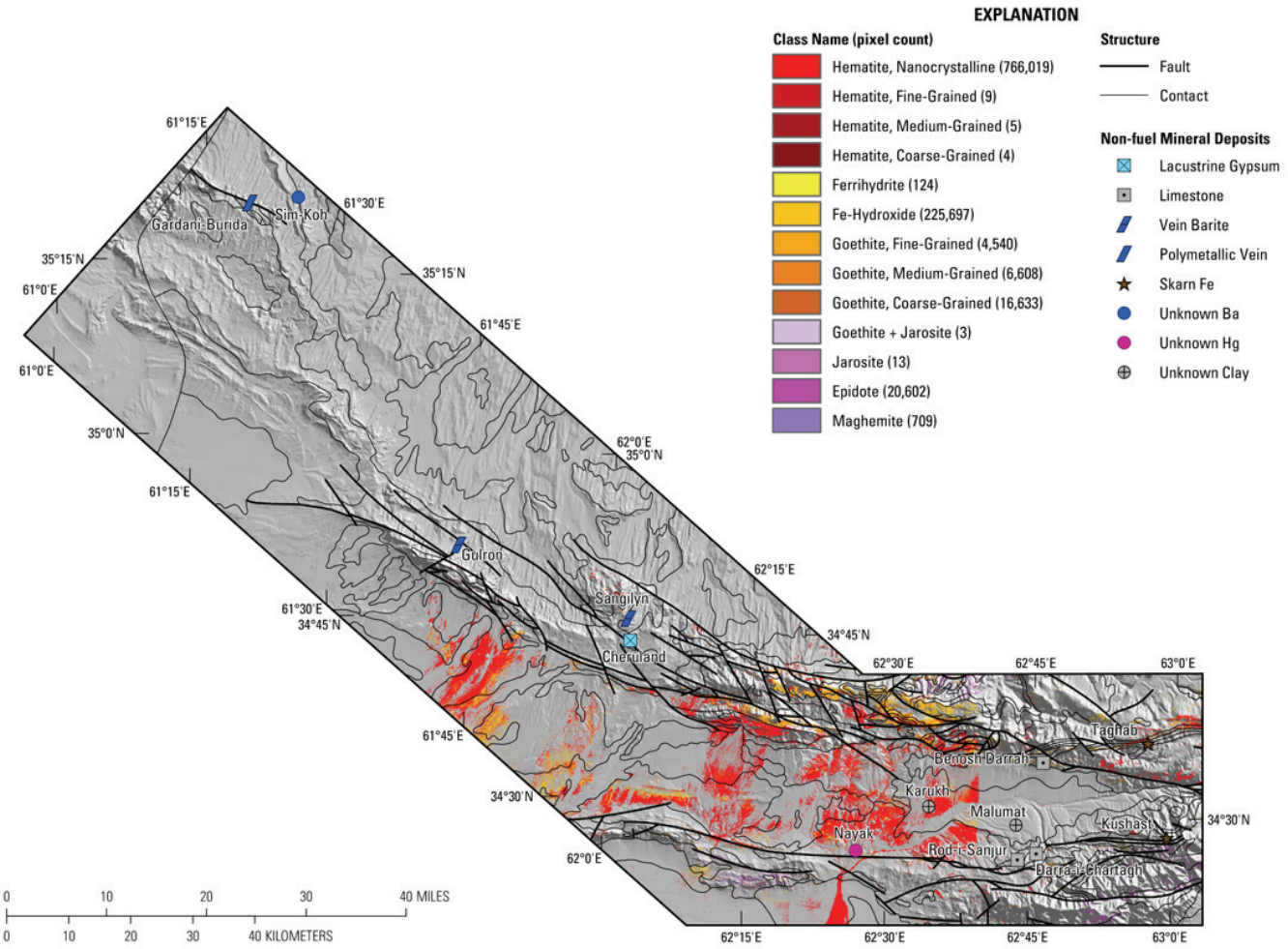

Figure 23B–10. Map of distribution of iron oxide and hydroxide derived from HyMap data in the North Herat area of interest.

23B.4.4 Common Alteration Minerals

Most of the minerals in this group are commonly present in hydrothermally altered rocks associated with epithermal mineral deposits (fig. 23B–11). Consequently, where they occur in distinct clusters is of great interest in terms of potential mineral deposits.

The largest occurrences of chlorite or epidote are found within the lower Tournaisian rocks in the southeast corner of the AOI. The eastern section of this occurrence terminates at a fault line. Smaller occurrences of chlorite or epidote are found within Lower Triassic rocks in the central region and are generally found along the geologic boundary of that unit, which is associated with a fault. In the south-central region, chlorite or epidote maps near a fault trace in Early Proterozoic rocks. The kaolinites primarily occur within Early Triassic age rocks in the central region and in Pennsylvanian age rocks in several locations. There are many faults within this area, and kaolinite does occur here and in several other areas along fault traces, especially along the northernmost fault complex. Here it can be found occurring along fault lines stretching from the western to eastern edge of the mapped area. The alunite and alunite + kaolinite classes occur in a large area within an Early Triassic age unit but also occur along fault lines throughout the faulted area to the north. The kaolinites and alunites map along these fault traces and may be associated with hydrothermal fluid flow along the faults making this an ideal area for additional geochemical and geophysical analysis. The largest occurrence is located near lat 34°39'00"N., long 62°12'05"E., and warrants further investigation.

Iron carbonates map in two regions within the AOI. One large occurrence is in Early Proterozoic rocks, and a second unit is mapped in several large clusters throughout the lower Tournaisian substage rocks and into adjacent Late Triassic intrusive rocks in the southeast corner of the AOI. The iron carbonates appear to map in older rock units, and several locations may be associated with a fault system. A special gypsum map was made and will be addressed in more detail in a separate section.

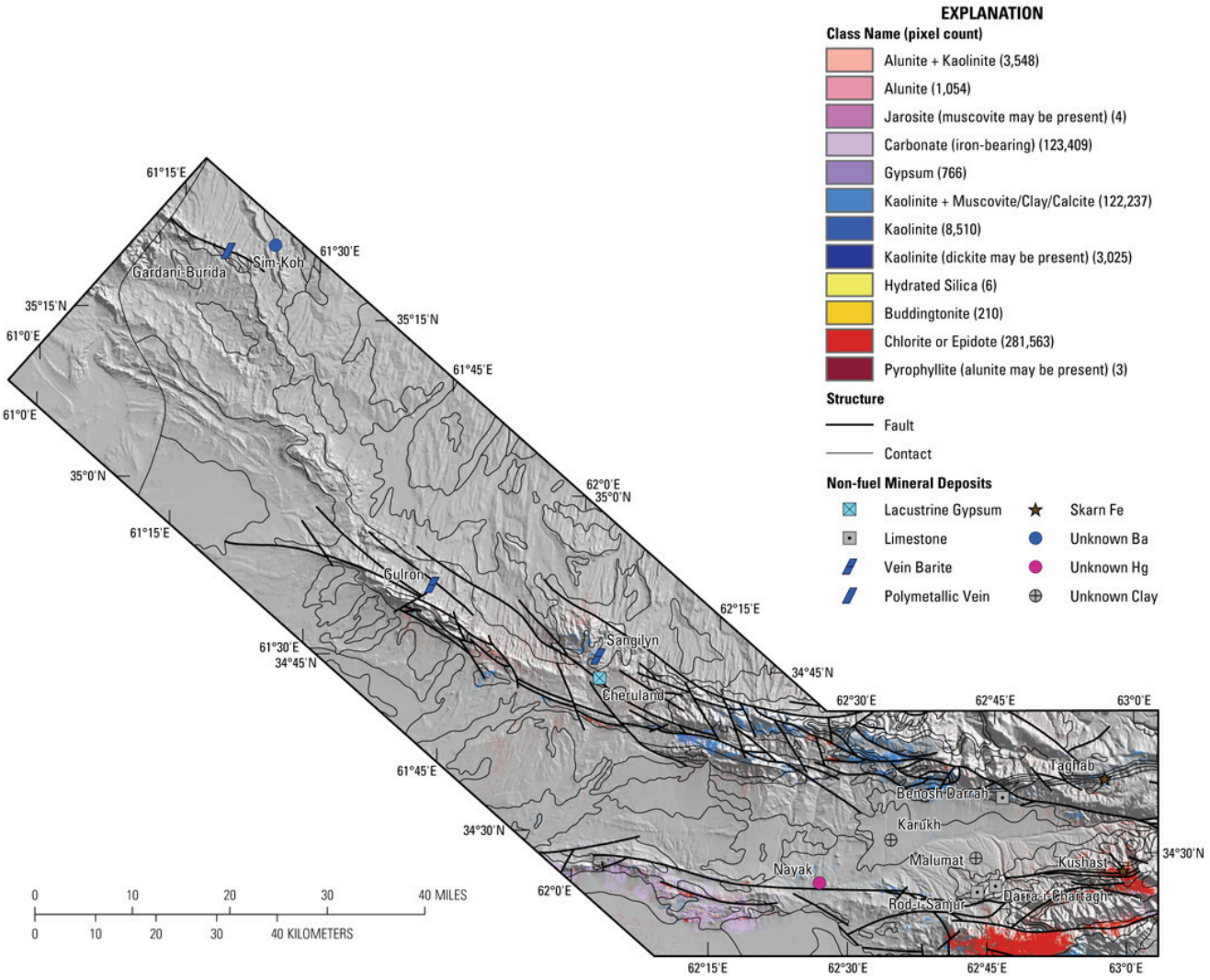

Figure 23B–11. Map of distribution of common alteration minerals derived from HyMap data in the North Herat area of interest.

23B34.5 Common Secondary Minerals

Secondary minerals, in the ‘Epidote’ and ‘Chlorite or Epidote’ classes (fig. 23B–12), are distributed throughout the AOI. The largest occurrences of chlorite or epidote are found within the lower Tournaisian rocks in the southeast corner of the AOI. Several areas of chlorite or epidote map along fault lines in the northern fault system. Chlorite or epidote also maps throughout the Early Proterozoic rocks and along a fault line. One small area of serpentines map in the southeast corner of the AOI.

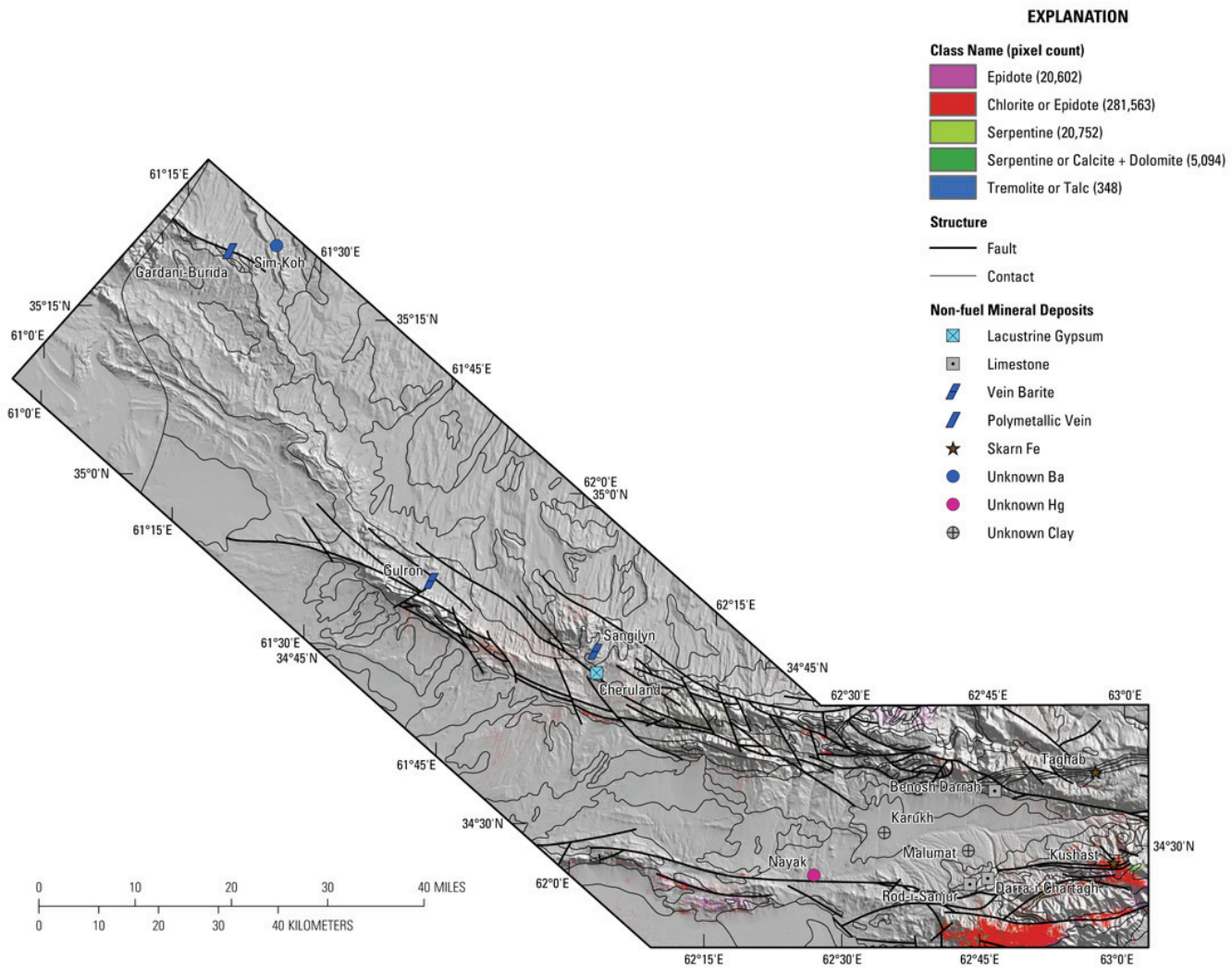

Figure 23B–12. Map of distribution of common secondary minerals derived from HyMap data in the North Herat area of interest.

23B.4.6 Gypsum

A MICA analysis using only gypsum in the list of reference spectra was conducted to expand the mapping of gypsum for greater detail. The result of that mapping is shown in figure 23B–13, in which gypsum is primarily distributed in the center of the North Herat AOI with concentrations of gypsum sparsely occurring to the northwest spanning nearly the entire area. Gypsum in this region generally occurs within upper Pliocene rocks that are described as containing gypsum (Peters and others, 2007; Abdullah and others, 1977). Gypsum was detected near the known gypsum occurrence of Cheruland and near the vein-barite prospect of Sangilyn. Additional concentrations of pixels with strong gypsum-related absorption features in their spectra occur near lat 34°35'38"N., long 62°25'46"E., over an area approximately 100 hectares in a narrow zone almost 4 km in length; these previously unreported gypsum concentrations in the center of the AOI are discussed in more detail in the anomaly map portion of this publication (King, Johnson, and others, 2011).

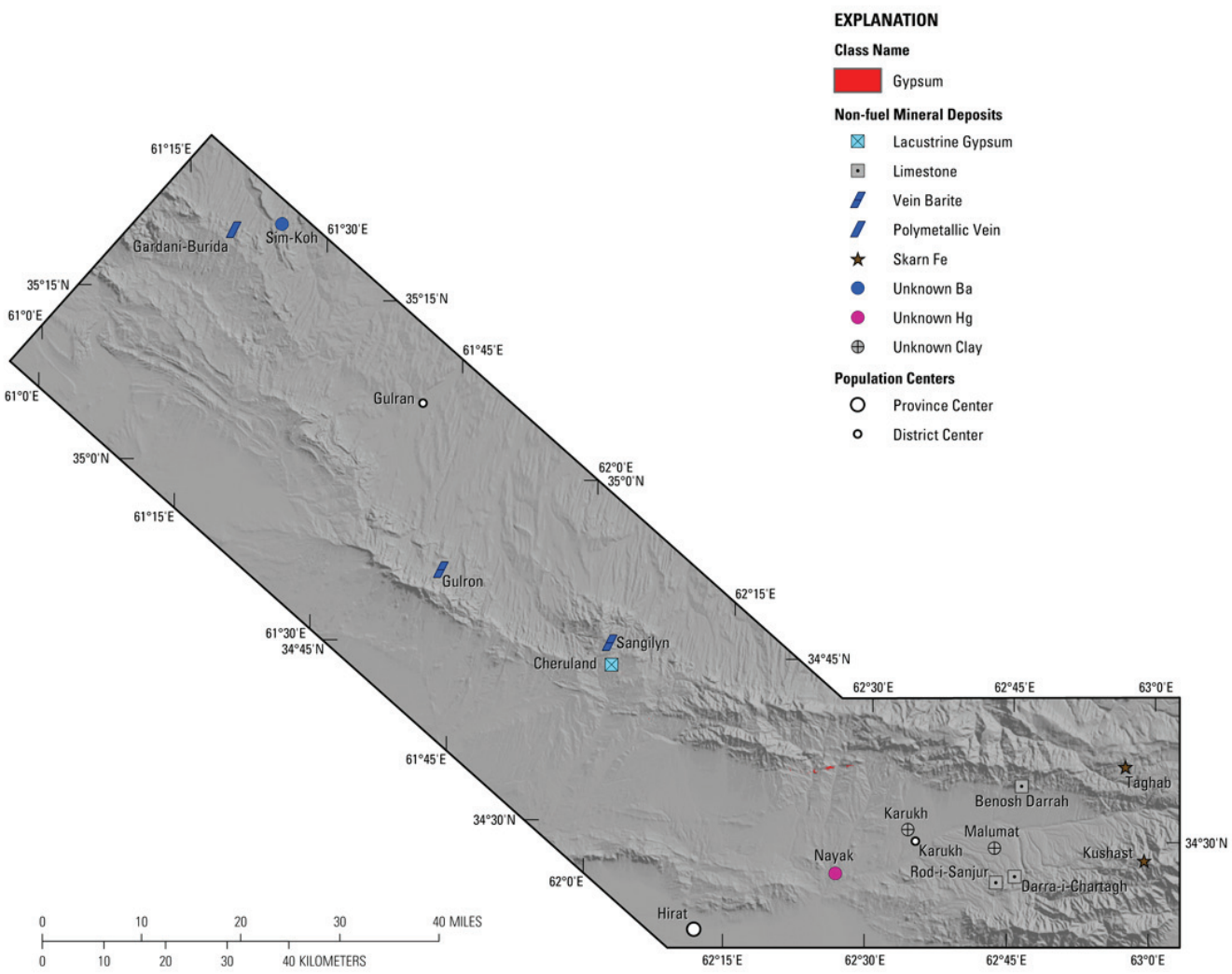

Figure 23B–13. (on previous page) Map of gypsum distribution derived from HyMap data in the North Herat area of interest.

23B.4.7 North Herat Subarea

Detailed maps of the North Herat subarea are presented in figures 23B–14 to 23B–25. The North Herat subarea covers more than 50 percent of the total HyMap coverage for the area, and most of the significant details of this area have already been discussed above. Figures 23B–14 to 18 show the index map, contrast-enhanced natural-color Landsat TM image, elevation data for this region, geologic map, and the geologic map with known mineral occurrences. The North Herat subarea, marked on figure 23B–14, covers 2,630 km^2. Of the 13 known mineral occurrences in the main Herat AOI, all but Gulron, Sim-Koh, Cheruland, Sangilyn, and Gardani-Burida occur in the North Herat subarea (see fig. 23B–18). Rocks in the North Herat subarea range in age from Recent to Early Proterozoic. Intrusive rocks of Proterozoic and Late Triassic age occur within the subarea. The Proterozoic intrusive rocks occur in the southeastern corner of the subarea. Permian and Mesozoic rocks tend to occur in the higher elevations in the north and eastern regions. Cenozoic rocks occur in the lower elevations in the western region and along the northern edge. Two fault systems occur in the subarea. Both fault systems are east-west trending along the northern and southern border.

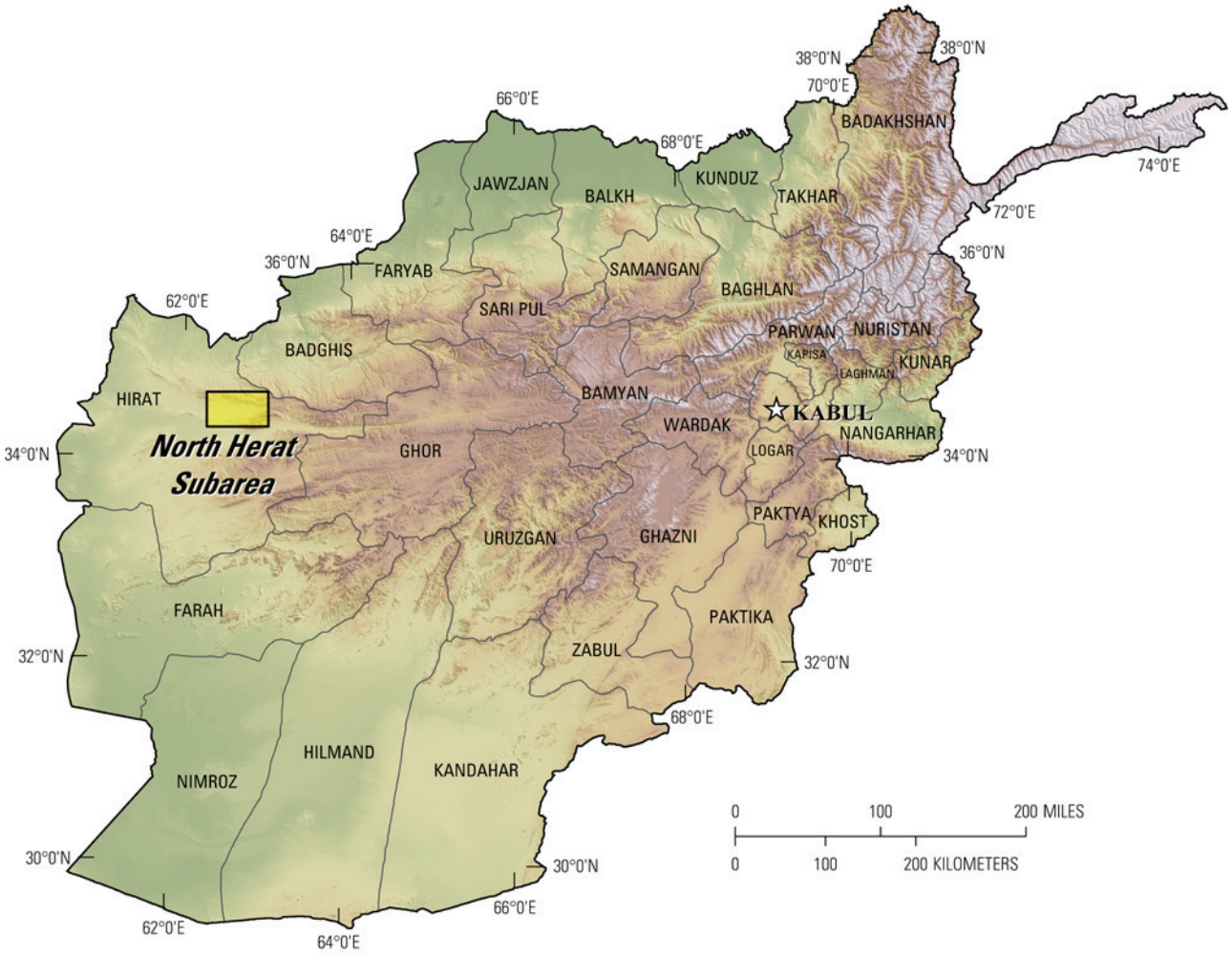

Figure 23B–14. Index map of the North Herat subarea, northeast Afghanistan.

Figure 23B–19 depicts the results of the MICA analyses of the HyMap data for the North Herat subarea for the 2-µm materials, which include clays, carbonates, phyllosilicates, sulfates, altered minerals, and other materials. The subarea is dominated by the calcite and calcite + clays/micas classes, which occur throughout the subarea and in most geologic units. Kaolinites and montmorillonite generally occur in the faulted terrain in the north and mostly occur within Triassic and Permian age rocks that are often faulted. Smaller concentrations of kaolinite are present along fault lines in the southern region of the subarea. The dolomite classes do not occur in a spatially consistent pattern in the subarea. Muscovite and illite map throughout the subarea and occur at some level in most geologic units. The largest occurrences of chlorite or epidote in the North Herat subarea are found in the southeast corner within the lower Tournaisian substage stratified rocks. Smaller spatially consistent patterns of chlorite or epidote are found within Lower Triassic rocks in the northwest region and the minerals are generally found along rock unit contacts and faults. Two concentrations of iron carbonate occur in the southwestern and southeastern corners of the subarea. The iron carbonate in the southwest corner is a small grouping of a much larger concentration (see fig. 23B–6). It may be associated with a fault running through Early Proterozoic rocks. In the eastern region, iron carbonates are associated with lower Tournaisian rocks. Large contiguous areas map along the southeastern edge of the subarea, but smaller groupings also occur within lower Tournaisian rocks along the southern border. As discussed in the gypsum section for the North Herat AOI, there is a large linear occurrence of gypsum that runs east-west in the northwestern corner of the subarea.

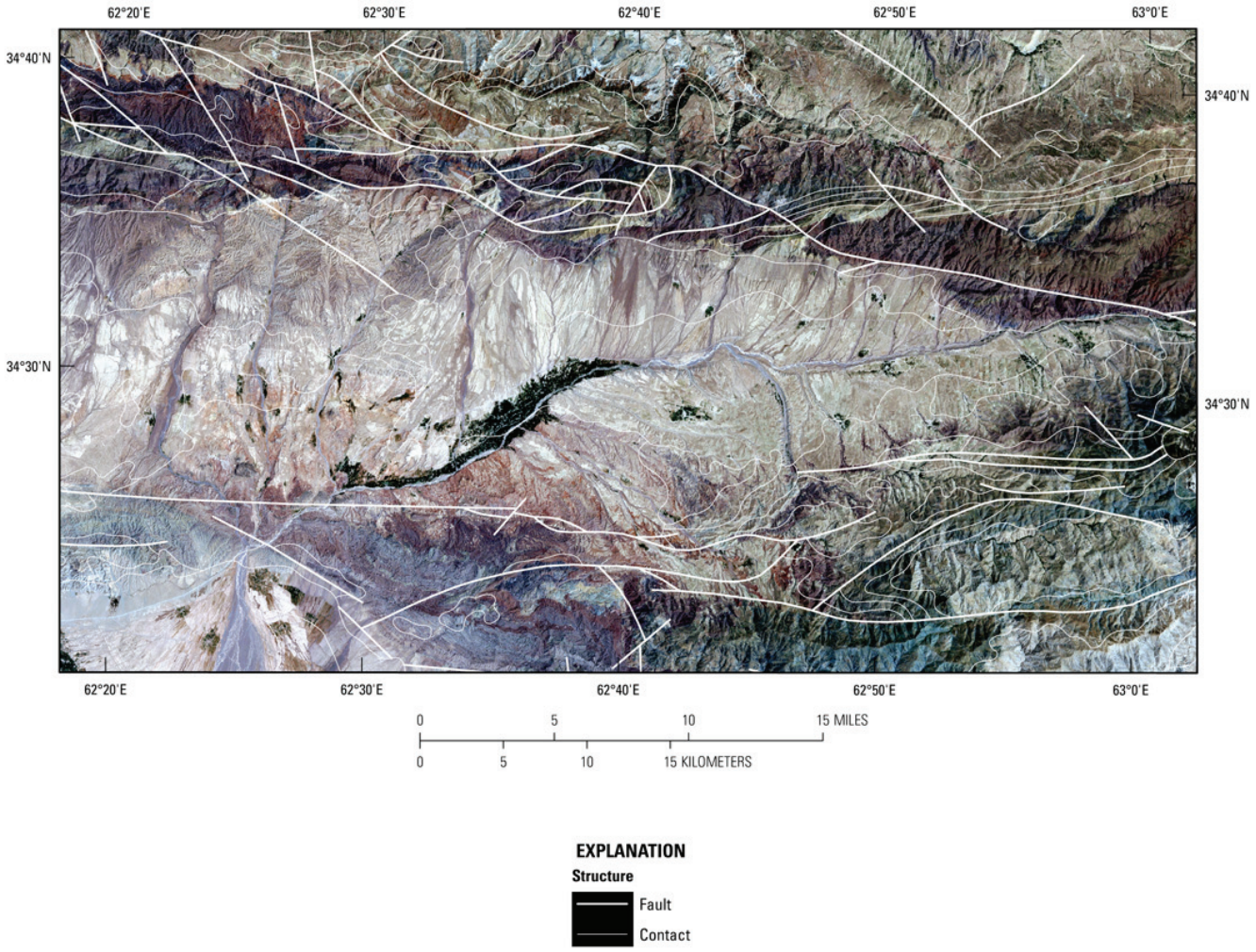

Figure 23B–15. Contrast-enhanced Landsat Thematic Mapper natural-color image of the North Herat subarea. Geologic contacts and faults from Doebrich and Wahl (2006) and Abdullah and Chmyriov (1977).

Figure 23B–20 shows the iron-bearing minerals for the North Herat subarea. Hematites are bounded by two fault systems and occur at lower elevations, with the exception of an occurrence in the eastern region that is associated with a fault line and rock unit contact. Fe^{2+} Fe^{3+} Type 2, Fe^{2+} Fe^{3+} Type 1, Fe^{2+} Type 1, and epidote map throughout the southern region of the subarea in many different geologic units. Fe-hydroxide and goethite map within the northern region along fault lines. Fe^{3+} Type 1 maps throughout the region in many contiguous clusters.

Figure 23B–21 shows the distribution of carbonate minerals that dominate this subarea. Here the calcite and calcite + clay/mica map in almost every unit. The two iron carbonate concentrations can also be seen.

Figure 23B–22 shows the distribution of clays and micas. Most of the muscovite and illite map south of the northern fault zone. Clays and micas that occur with carbonates map throughout the subarea. The chlorite or epidote class can clearly be seen in the southeast region with minor clusters on the northwest. Kaolinites are mapped along fault traces in the northwestern region.

The iron-oxides and hydroxides map (fig. 23B–23) shows large detections of iron hydroxide, goethite, and hematite. The iron-hydroxide and goethite classes appear to be associated with kaolinites and fault traces.

Figure 23B–24 represents the common alteration minerals and shows detections of chlorite or epidote, kaolinites, and iron carbonates. Also located in this subarea is a linear concentration of gypsum, which was discussed in the gypsum section.

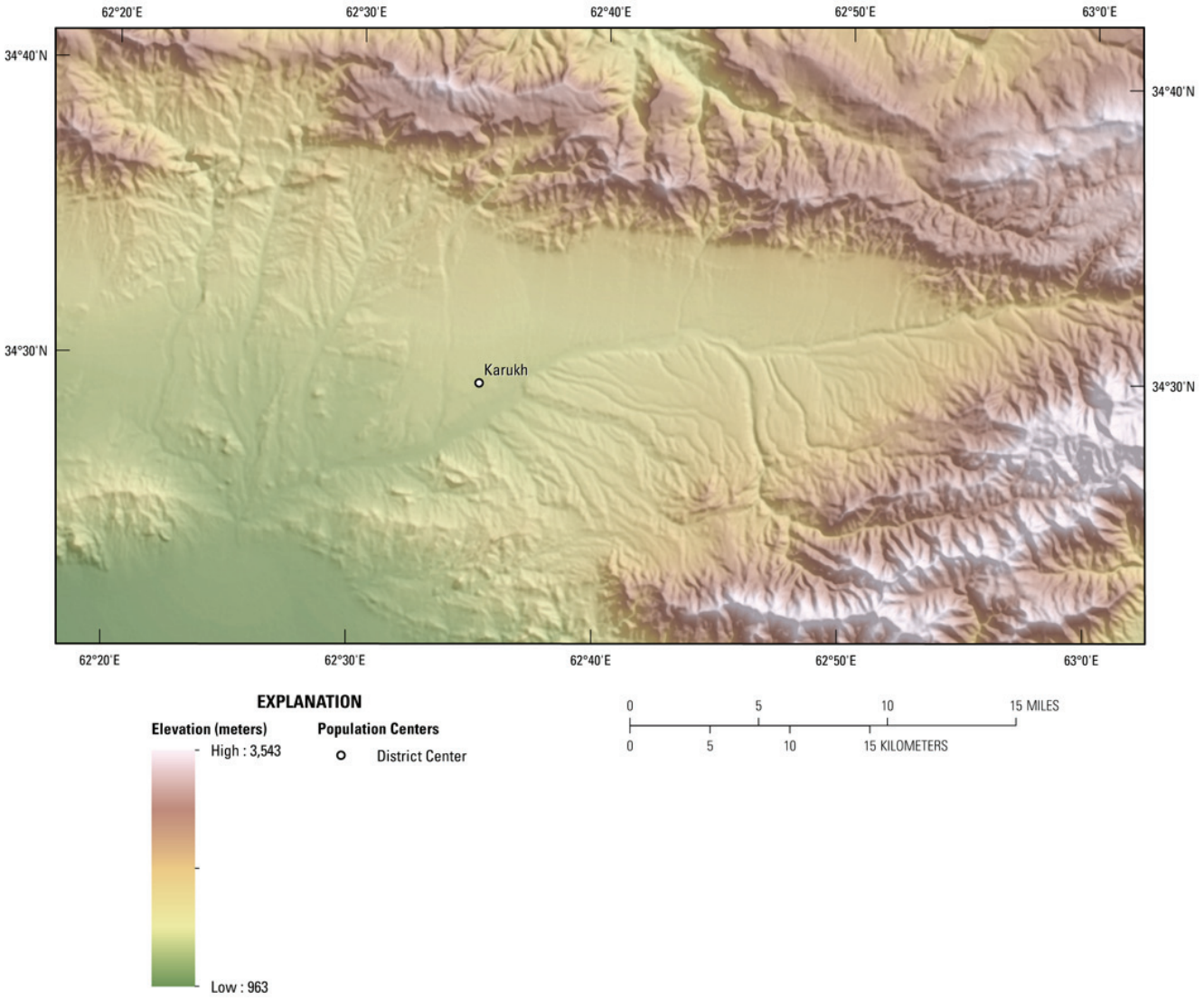

Figure 23B–16. Elevations and topography of the North Herat subarea.

Figure 23B–25 shows the common secondary minerals. The epidote, epidote or chlorite, and serpentine classes are shown within this region.

23B.5 Summary

The HyMap data cover the southeastern part of the AOI, including 10 of the 13 known mineral occurrences. Carbonate class minerals cover most of the North Herat AOI. Muscovites and illites were detected over large areas of the AOI. A large concentration of muscovite is found within Triassic intrusive rocks in the southeast corner of the region. Epidote and chlorite were found in spatially consistent patterns in large areas in the southeast and smaller groupings throughout the AOI. Most of the chlorite or epidote is detected in lower Tournaisian rocks in the southeast region. Many other chlorite or epidote detections are found along fault lines in the northern fault system. Kaolinites were generally mapped in Lower Triassic rocks with smaller groupings in Pennsylvanian rocks. The presence of kaolinites is frequently associated with hydrothermal processes. Occurrences are of increased interest if they are associated with faulting (pathways for fluid flow) and (or) exhibit well-defined patterns of distribution (which may be indicative of structural control). Well-defined concentrations of alunite, kaolinite, goethite, alunite, and Fe-hydroxide material occur throughout the northern fault system in the North Herat AOI. A concentration located near lat 34°39'00"N., long 62°12'05"E., contains kaolinite and

kaolinite + alunite and should be looked at in more detail, as well as several smaller areas along the northern fault lines. Iron carbonates map in two separate concentrations. A large occurrence is mapped in Early Proterozoic rocks in the south-central region and another area is mapped with lower Tournaisian substage rocks in the southeast region.

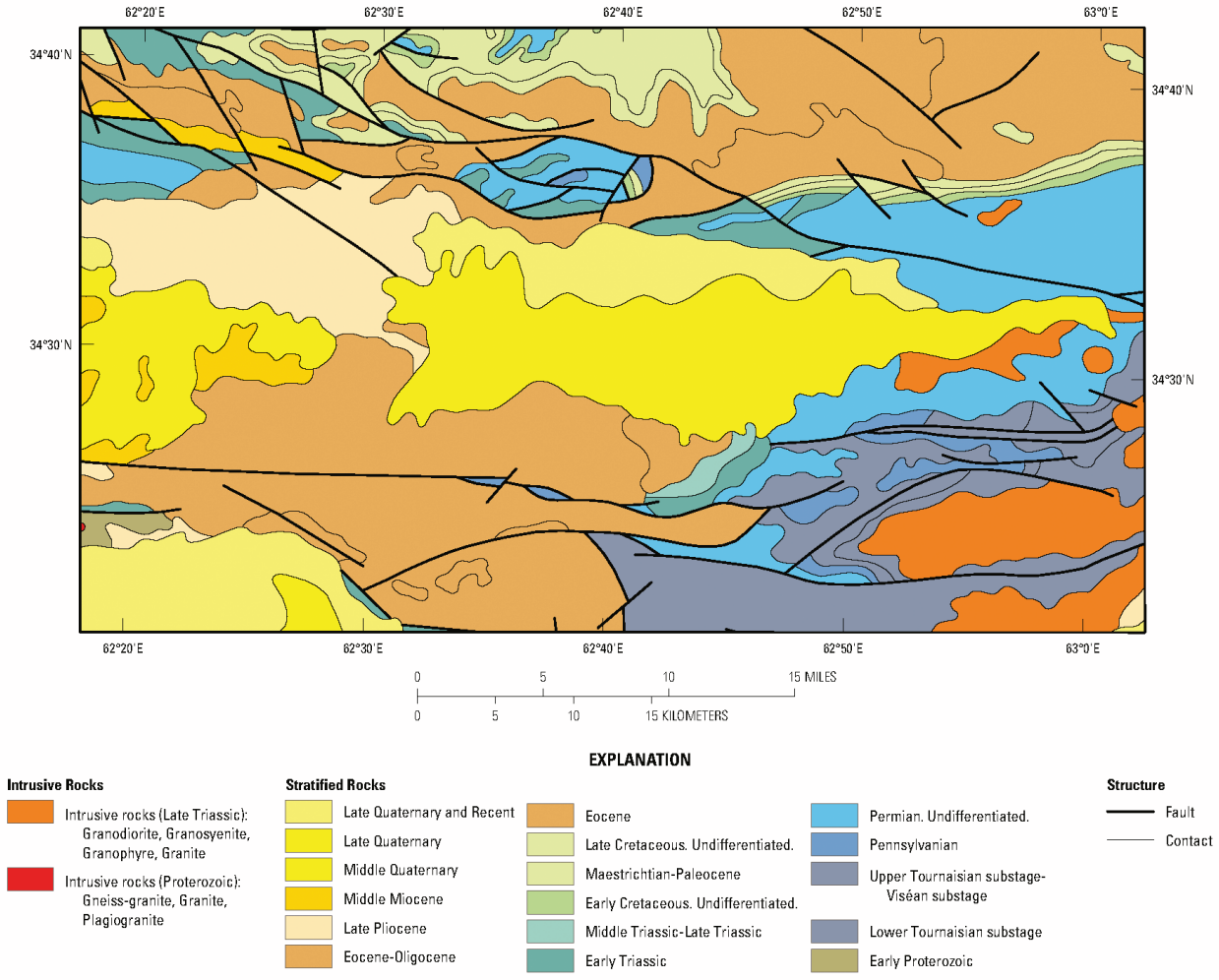

Figure 23B–17. Geologic map of the North Herat subarea from the geologic map of Afghanistan (Doebrich and Wahl, 2006; Abdullah and Chmyriov, 1977).

The hematites are bounded by the two east-west trending fault systems in rocks at lower elevations. Goethite and Fe-hydroxide material occur throughout the northern fault system in the North Herat AOI. The Fe^{2+} Fe^{3+} Type 2, Fe^{2+} Fe^{3+} Type 1, and Fe^{2+} Type 1 classes map within the southern fault system.

A special gypsum MICA analysis was performed to map the gypsum detections in greater detail. The analysis yielded detections consistent with known gypsum occurrences at Cheruland. Several previously unknown concentrations of pixels were detected that warrant additional investigation. Although barite spectra lack diagnostic spectral bands, gypsum is mapped in the vicinity of the Sangilyn vein-barite prospect and may be associated with this deposit type. The gangue minerals for this prospect are listed as quartz and calcite, and the HyMap data does show that the mineral occurrence is located in calcite-rich rocks.

The rest of the known mineral occurrences occur both in the main North Herat AOI and in the North Herat subarea. The limestone known mineralized areas of Benosh Darrah, Darra-i-Chartagh, and Rod-i-Sanjur map within calcite-class minerals and are consistent with these types of prospects. The Karukh and Malumat clay prospects map within contiguous areas of calcite + montmorillonite.

Montmorillonite is also mapped throughout the area but in a much more scattered pattern. The Kushast and Taghab iron-skarn mineral occurrences may be associated with Fe^{2+} Fe^{3+} Type 2 minerals at Kushast and Fe^{3+} Type 1 minerals at Taghab.

The HyMap data for the North Herat area show several locations with specific minerals (alunite) or groups of minerals (alunite+kaolinite) that might be related to hydrothermal alteration and metal deposition and suggest the need for additional field sampling, geophysical and geochemical characterization.

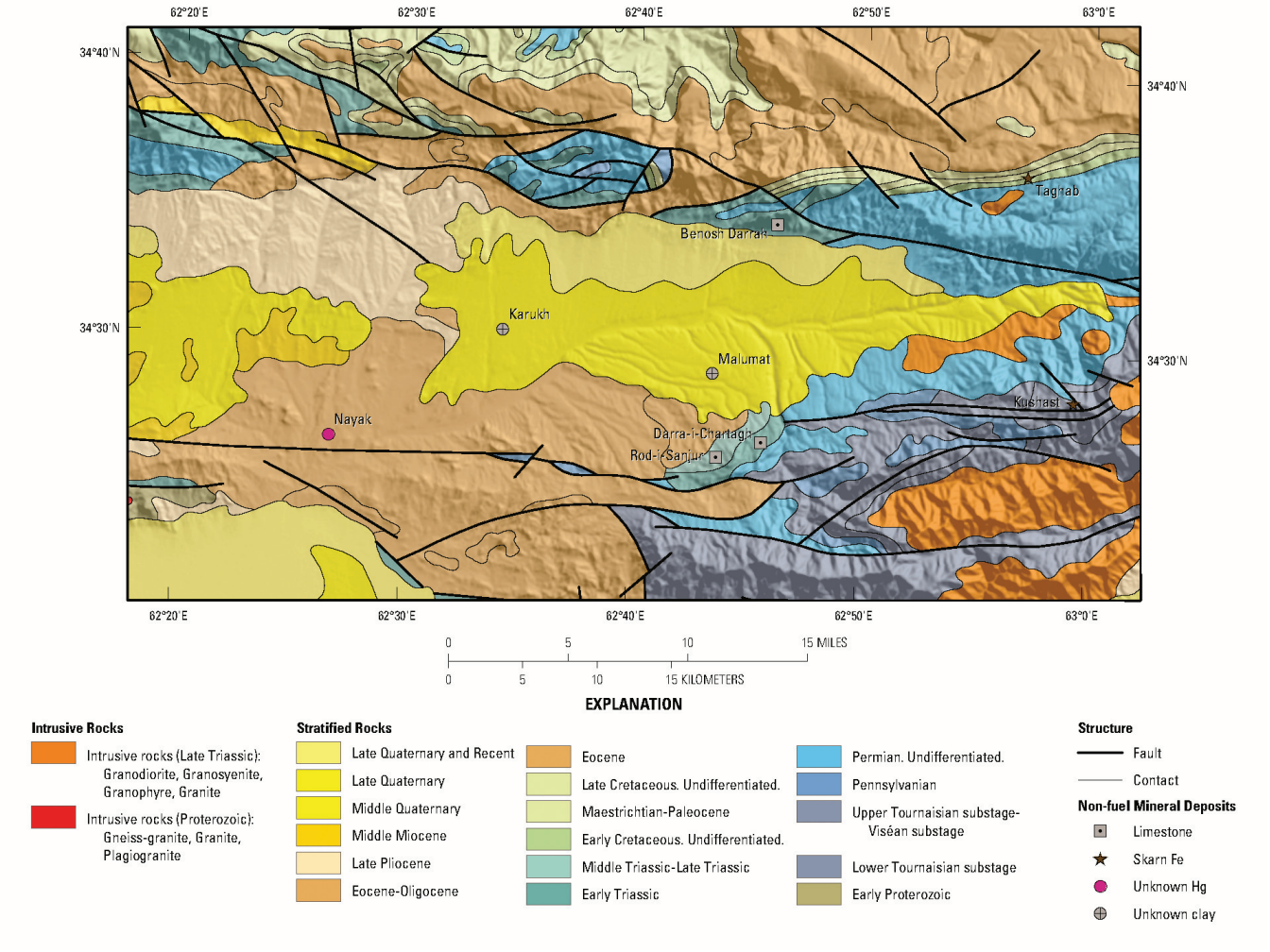

Figure 23B–18. Sites of known mineralization by deposit type (Peters and others, 2007) on the geologic map of the North Herat subarea from the geologic map of Afghanistan (Doebrich and Wahl, 2006; Abdullah and Chmyriov, 1977).

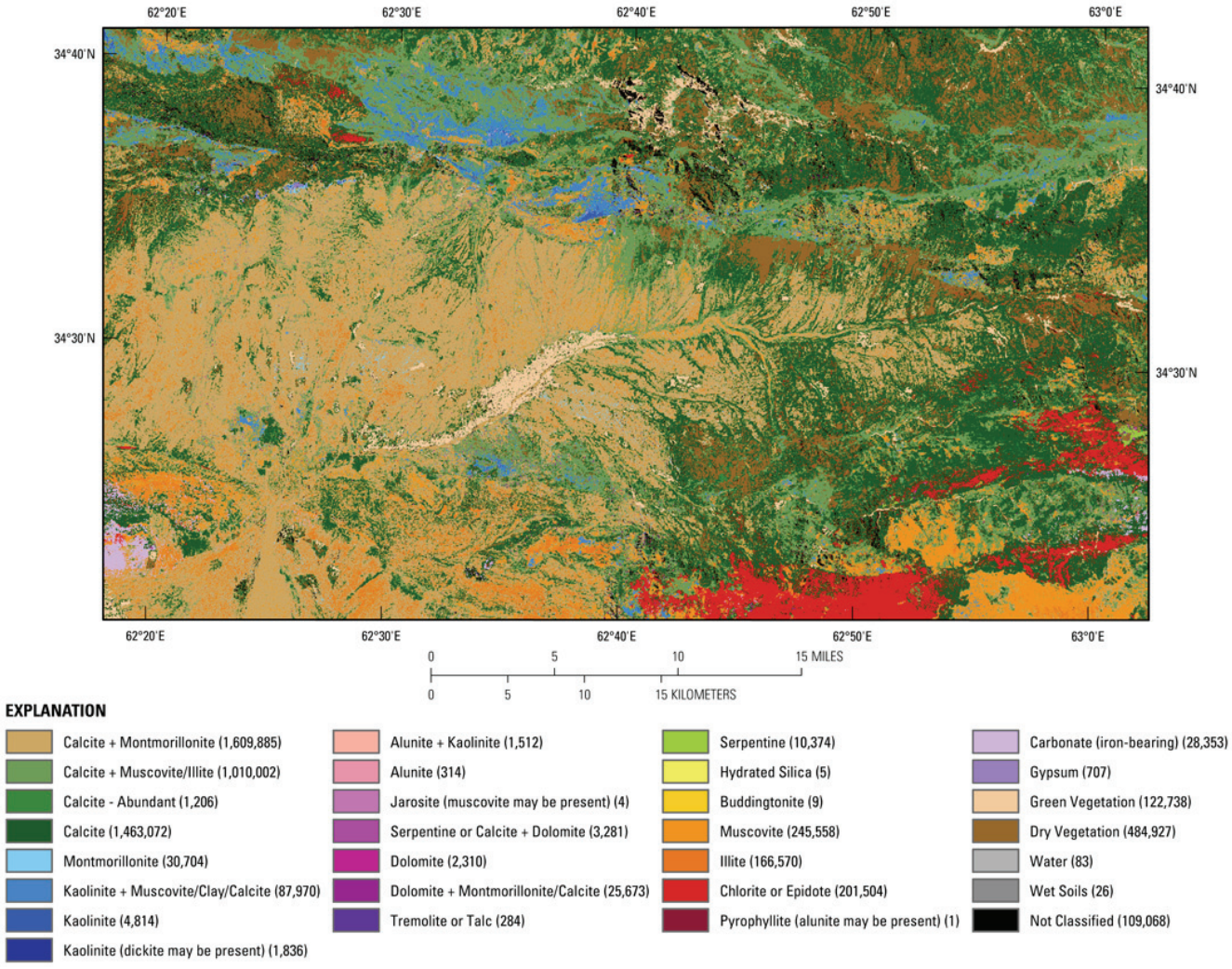

Figure 23B–19. Map of carbonates, phyllosilicates, sulfates, altered minerals, and other materials derived from HyMap data in the North Herat subarea.

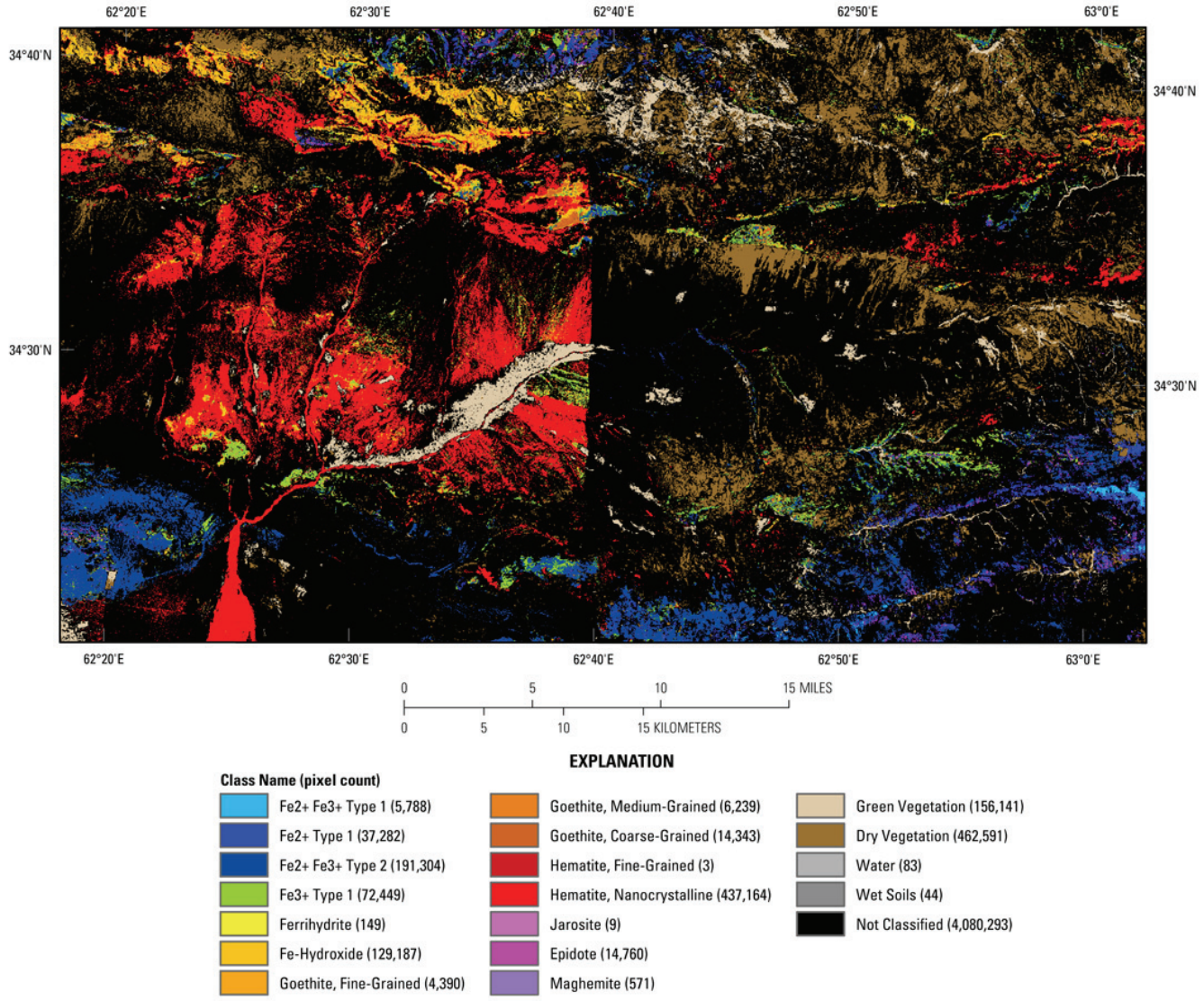

Figure 23B–20. Map of iron-bearing minerals and other materials derived from HyMap data in the North Herat subarea.

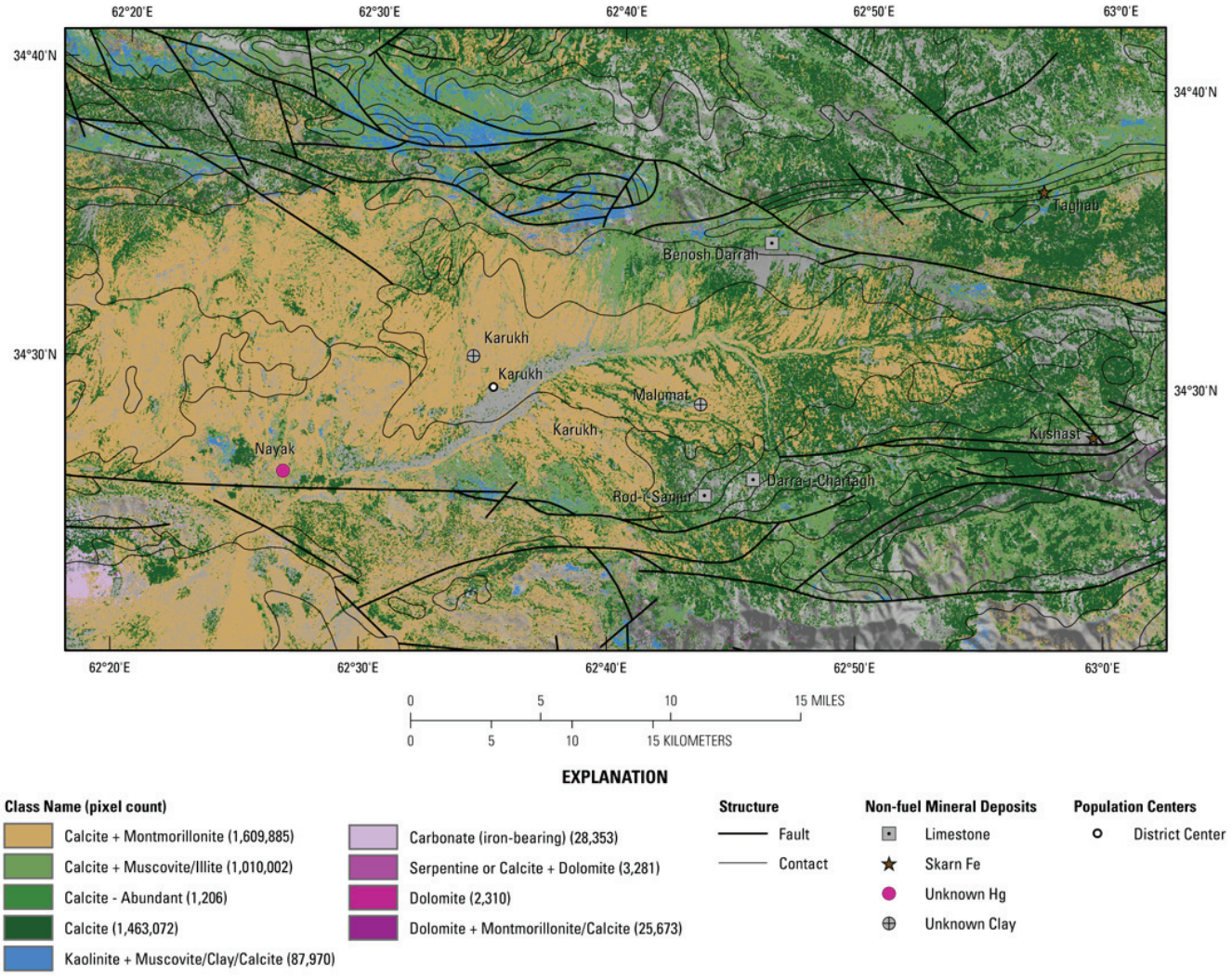

Figure 23B–21. Map of distribution of carbonate minerals derived from HyMap data in the North Herat subarea.

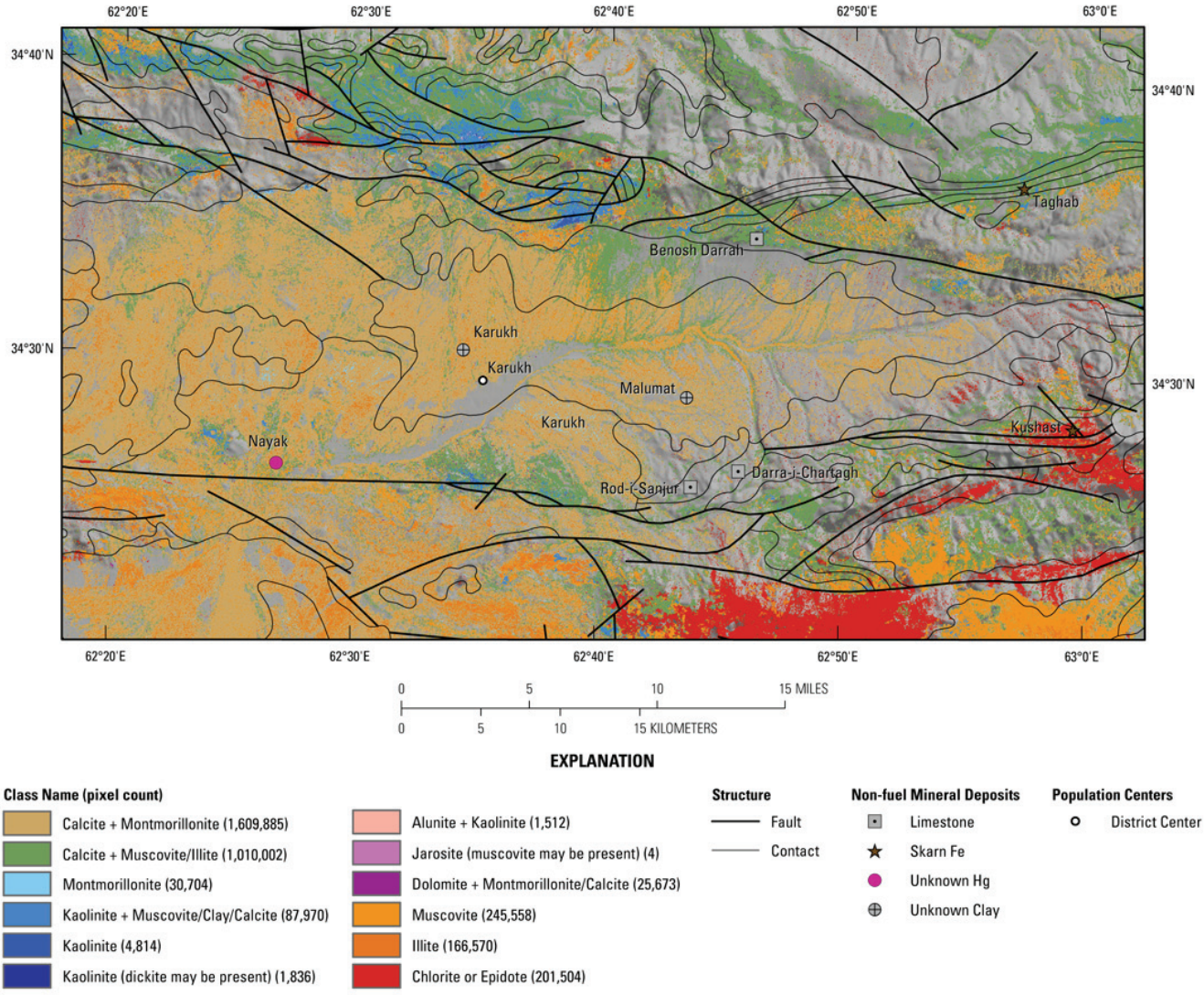

Figure 23B–22. Map of distribution of clay and mica minerals derived from HyMap data in the North Herat subarea.

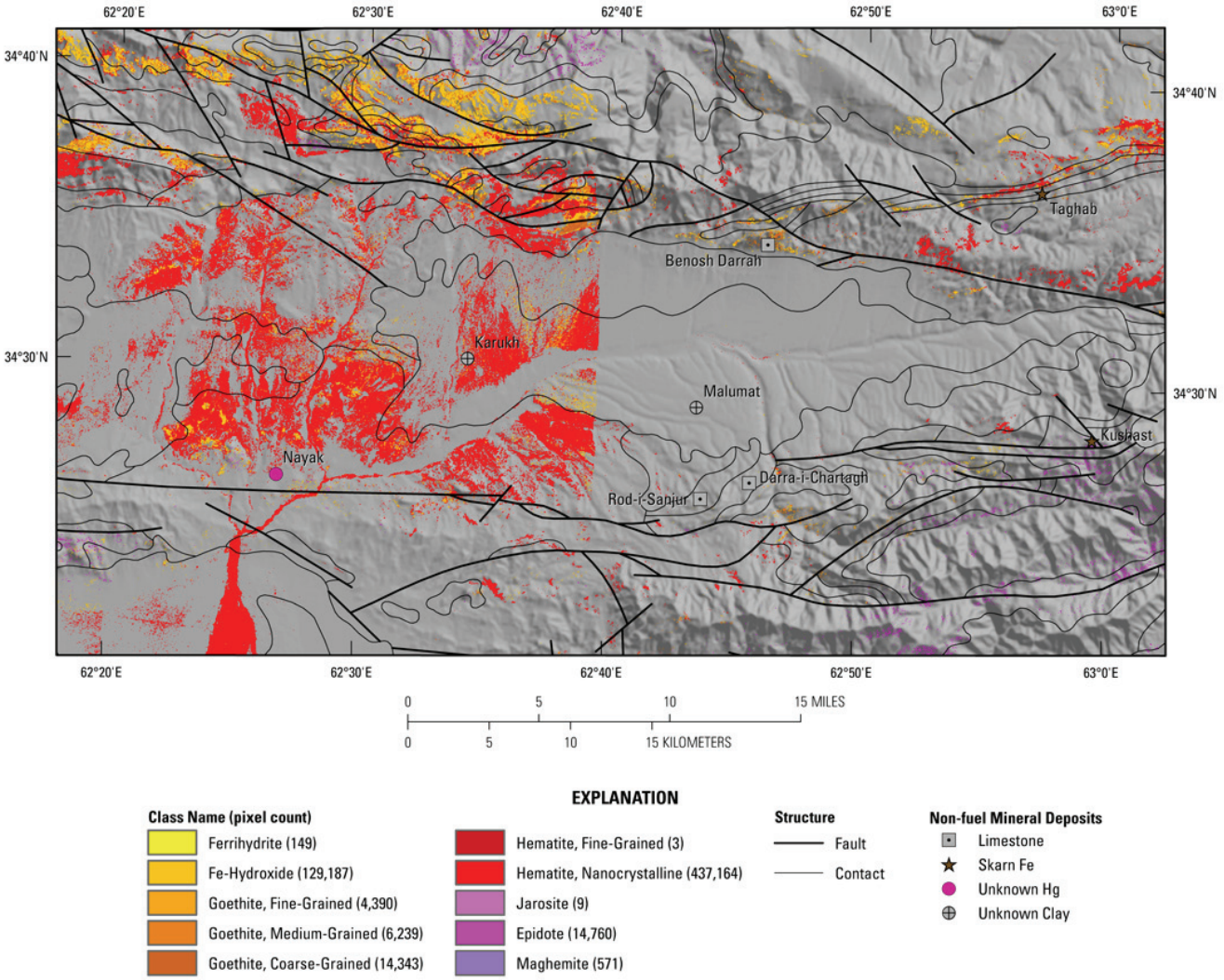

Figure 23B–23. Map of distribution of iron oxide and hydroxide derived from HyMap data in the North Herat subarea.

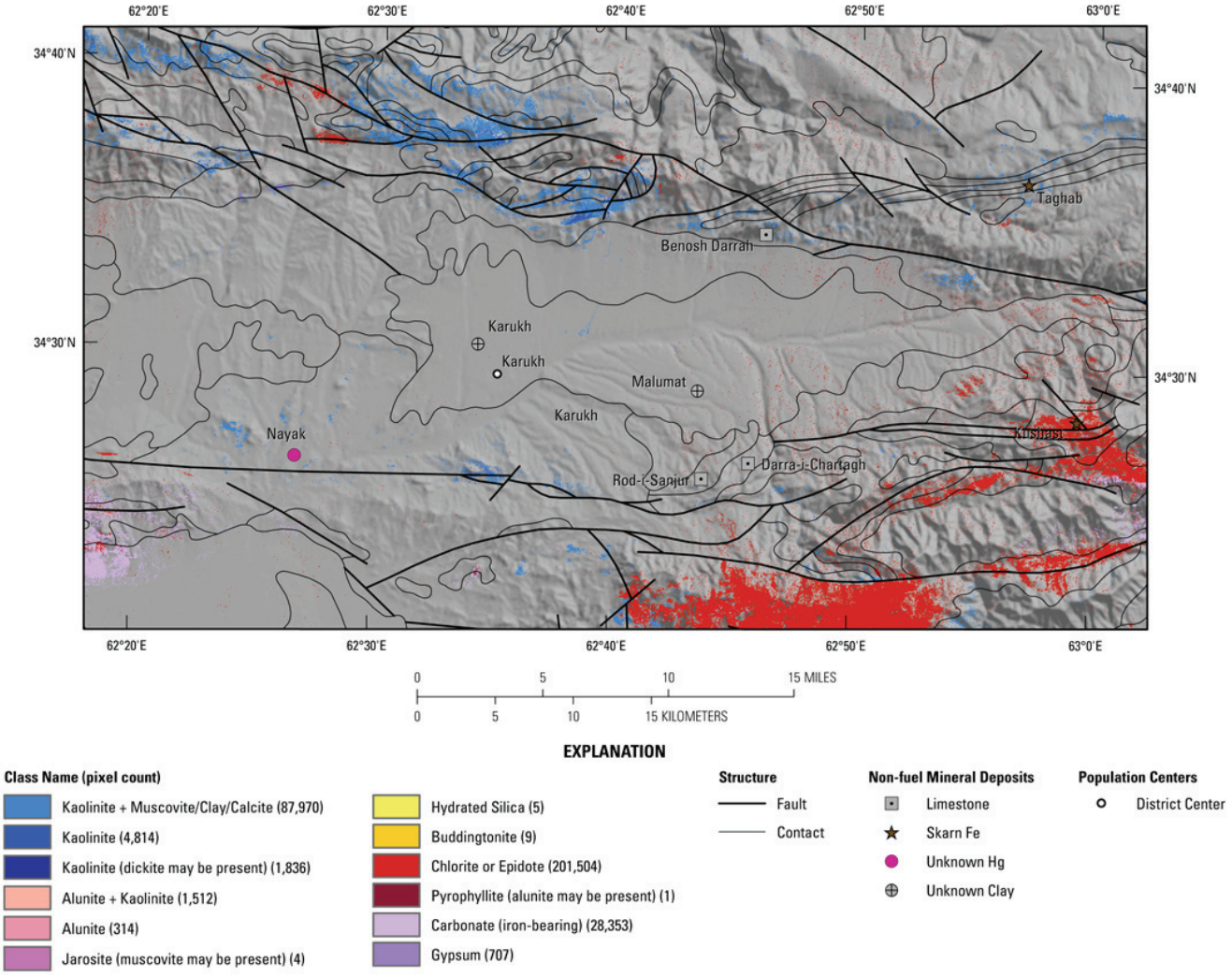

Figure 23B–24. Map of distribution of common alteration minerals derived from HyMap data in the North Herat subarea.

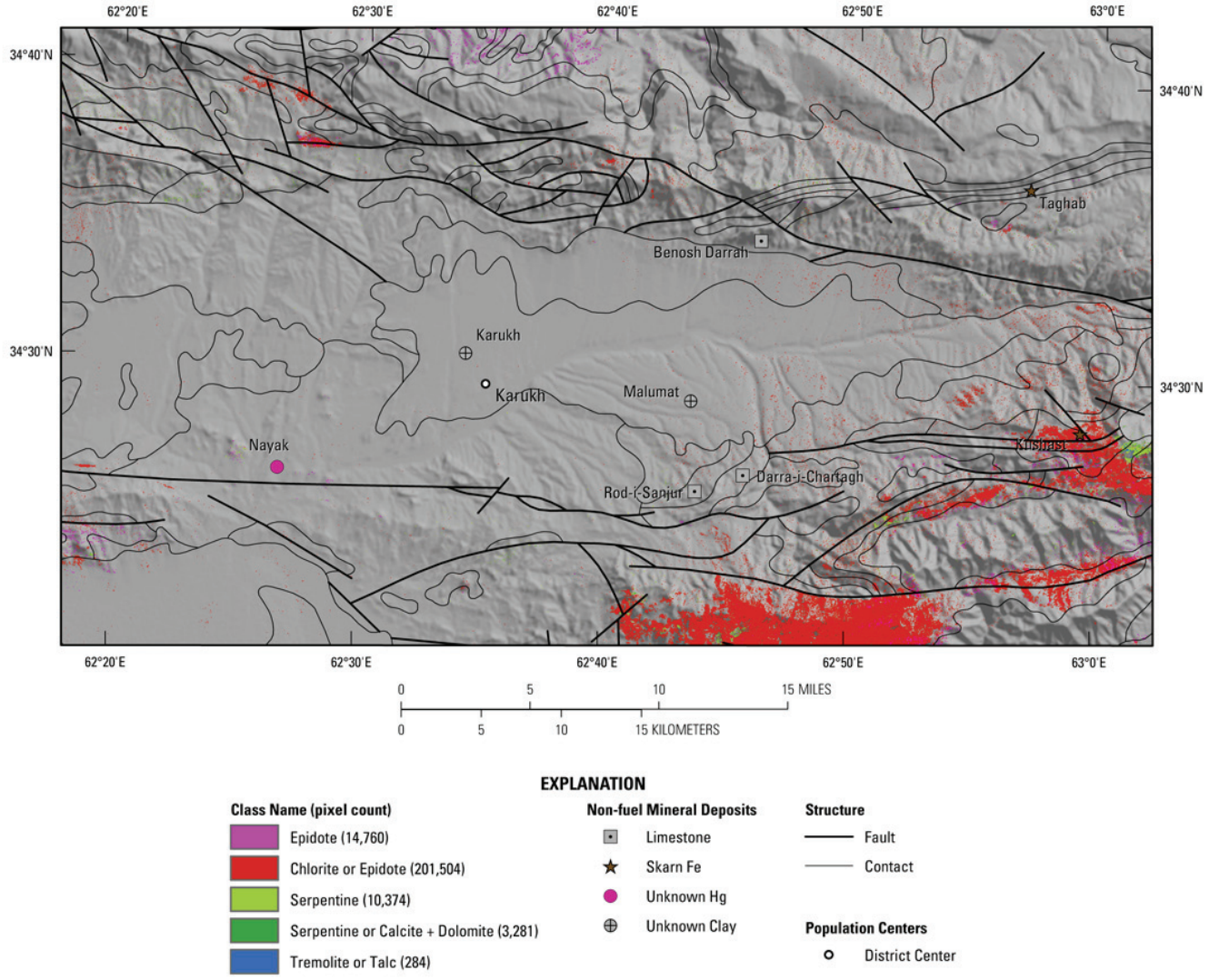

Figure 23B–25. Map of distribution of common secondary minerals derived from HyMap data in the North Herat subarea.

23B.6 References Cited

Abdullah, Sh., and Chmyriov, V.M., 1977, Geological map of Afghanistan: Kabul, Afghanistan, Ministry of Mining and Industry of Democratic Republic of Afghanistan, scale 1:500,000.

Abdullah, Sh., Chmyriov, V.M., Stazhilo-Alekseev, K.F., Dronov, V.I., Gannan, P.J., Rossovskiy, L.N., Kafarskiy, A.Kh., and Malyarov, E.P., 1977, Mineral resources of Afghanistan (2d ed.): Kabul, Afghanistan, Republic of Afghanistan Geological and Mineral Survey, 419 p.

Cocks, T., Jenssen, R., Stewart, A., Wilson, I., and Shields, T., 1998, The HyMap airborne hyperspectral sensor—The system, calibration and performance, *in* Schaepman, M., Schlapfer, D., and Itten, K.I., eds., Proceedings of the 1st EARSeL Workshop on Imaging Spectroscopy, 6–8 October 1998, Zurich: Paris, European Association of Remote Sensing Laboratories, p. 37–43.

Davis, P.A., 2007, Landsat ETM+ false-color image mosaics of Afghanistan: U.S. Geological Survey Open-File Report 2007–1029, 22 p. (Also available at *http://pubs.usgs.gov/of/2007/1029/*.)

Doebrich, J.L., and Wahl, R.R., comps., *with contributions by* Doebrich, J.L., Wahl, R.R., Ludington, S.D., Chirico, P.G., Wandrey, C.J., Bohannon, R.G., Orris, G.J., Bliss, J.D., and _____, 2006, Geologic and mineral resource map of Afghanistan: U.S. Geological Survey Open File Report 2006–1038, scale 1:850,000, available at *http://pubs.usgs.gov/of/2006/1038/*.

Hoefen, T.M., Kokaly, R.F., and King, T.V.V., 2010, Calibration of HyMap data covering the country of Afghanistan, *in* Proceedings of the 15th Australasian Remote Sensing and Photogrammetry Conference, Alice Springs, Australia, September 12–17, 2010, p. 409, available at *http://dl.dropbox.com/u/81114/15ARSPC-Proceedings.zip/*.

King, T.V.V., Kokaly, R.F., Hoefen, T.M., and Knepper, D.H., 2010, Resource mapping in Afghanistan using HyMap data, *in* Proceedings of the 15th Australasian Remote Sensing and Photogrammetry Conference, Alice Springs, Australia, September 12–17, 2010, p. 500, available at *http://dl.dropbox.com/u/81114/15ARSPC-Proceedings.zip/*.

King, T.V.V., Johnson, M.R., Hoefen, T.M., Kokaly, R.F., and Livo, K.E., 2011, Mapping potential mineral resource anomalies using HyMap data, *in* King, T.V.V., Johnson, M.R., Hubbard, B.E., and Drenth, B.J., eds, Identification of mineral resources in Afghanistan—Detecting and mapping resource anomalies in prioritized areas using geophysical and remote sensing (ASTER and HyMap) data in Afghanistan: U.S. Geological Survey Open-File Report 2011–1229, available at *http://pubs.usgs.gov/of/2011/1229/*.

King, T.V.V., Kokaly, R.F., Hoefen, T.M., Dudek, K. and Livo, K.E., 2011, Surface materials map of Afghanistan—Iron-bearing minerals and other materials: U.S. Geological Survey Scientific Investigations Map 3152–B.

Kokaly, Ray, 2011, PRISM—Processing routines in IDL for spectroscopic measurements: U.S. Geological Survey Open-File Report 2011–1155, available at *http://pubs.usgs.gov/of/2011/1155/*.

Kokaly, R.F., King, T.V.V., and Livo, K.E., 2008, Airborne hyperspectral survey of Afghanistan 2007—Flight line planning and HyMap data collection: U.S. Geological Survey Open-File Report 2008–1235, 14 p.

Kokaly, R.F., King, T.V.V., Hoefen, T.M., Dudek, K. and Livo, K.E., 2011, Surface materials map of Afghanistan—Carbonates, phyllosilicates, sulfates, altered minerals, and other materials: U.S. Geological Survey Scientific Investigations Map 3152–A.

Peters, S.G., Ludington, S.D., Orris, G.J., Sutphin, D.M., Bliss, J.D., and Rytuba, J.J., eds., and the U.S. Geological Survey-Afghanistan Ministry of Mines Joint Mineral Resource Assessment Team, 2007, Preliminary non-fuel mineral resource assessment of Afghanistan: U.S. Geological Survey Open-File Report 2007–1214, 810 p., 1 CD–ROM. (Also available at *http://pubs.usgs.gov/of/2007/1214/*.)